Boundary Integral Formulations for Flexural Wave Scattering in Thin Plates

Peter Nekrasov^{a,*}, Tim Su^a, Travis Askham^b, Jeremy G. Hoskins^a

^aCommittee on Computational and Applied Mathematics, University of Chicago, 5747 S. Ellis
Avenue, 60637, Chicago, IL, USA

^bDepartment of Mathematical Sciences, New Jersey Institute of Technology, Cullimore
Hall, 07102, Newark, NJ, USA

Abstract

In this paper we develop second kind integral formulations for flexural wave scattering problems involving the clamped, free, and supported plate boundary conditions. While the clamped plate problem can be solved with layer potentials previously developed for the biharmonic equation [1], the free plate problem is more difficult due to the complex nature of the boundary conditions. In this paper we describe a representation for the free plate problem that uses the Hilbert transform to cancel singularities of certain layer potentials, ultimately leading to a Fredholm integral equation of the second kind. Additionally, for the supported plate problem, we improve on an existing representation to obtain a second kind integral equation. With these representations, it is possible to solve flexural wave scattering problems with high-order-accurate methods, examine the far-field patterns of scattering objects, and solve large problems involving multiple scatterers.

Keywords: Integral equations, biharmonic, elasticity, Hilbert transform, fast algorithms

1. Background

Scientific interest in the vibrations of free plates can be traced as far back as Ernst Chladni's famous demonstration in front of Napoleon at the Paris Academy in 1808. In the century that followed, the theory of plates developed rapidly through the work of Kirchhoff [2] and Love [3] and was later refined and popularized by Timoshenko [4]. Today, this theory is applied to the modeling and observation of elastic waves in many engineering and geophysics contexts. These vibrations, known as flexural waves, were responsible for bringing down the Tacoma Narrows Bridge [5], while the same vibrations led to substantial calving in the Larsen A and B and Wilkins ice shelves [6]. In short, flexural phenomena pose a significant challenge to the integrity of both the natural and built environments.

Email address: pn3@uchicago.edu (Peter Nekrasov)

^{*}Corresponding author.

Flexural waves are typically modelled by the thin plate approximation, where the vertical displacement of a plate is defined as a scalar function of two horizontal dimensions. For some closed subset of the plane $\Omega \subset \mathbb{R}^2$ and $\mathbf{x} := (x, y) \in \Omega$, the out-of-plane displacement $u(\mathbf{x})$ is described by the following fourth-order partial differential equation (PDE):

$$\Delta^2 u - k^4 u = 0 \qquad \text{on } \Omega \tag{1}$$

where $\Delta^2 u := \frac{\partial^4 u}{\partial x^4} + 2 \frac{\partial^4 u}{\partial x^2 \partial y^2} + \frac{\partial^4 u}{\partial y^4}$ is the biharmonic operator and k is the wavenumber. The first term in the equation corresponds to a bending force, while the second term represents the inertia after assuming that the solution is harmonic in time. Equation (1) can also be thought of as an eigenvalue problem corresponding to the biharmonic operator.

Since equation (1) is fourth-order, two boundary conditions (BCs) are required to fully determine the problem. In the present work, we are concerned with the three sets of boundary conditions that arise most frequently in thin plate theory: the clamped, free, and supported plates [4, 7, 8, 9, 10]. The clamped plate BCs restrict the motion of the plate at the boundary by fixing both the displacement and slope, while the free plate BCs prescribe bending and shear forces, allowing the displacement and slope to oscillate at the boundary. Lastly, the supported plate restricts displacement but allows for sloping, leading to a combination of fixed and flexible behavior. The precise description for these boundary conditions, as well as examples of where they arise, are given in Sections 3, 4, and 5.

There are many physical reasons to study exterior problems involving these boundary conditions. Plates that are found in buildings and bridges may be supported from within by internal columns, rods, and springs that affect their flexure [11]. Alternatively, cut-outs can also made to these plates to lighten or ventilate the structure [12, 13]. These inclusions are often used to alter or eliminate resonant modes [14, 15]. This is valuable in the field of acoustics, where one is typically searching for a very specific frequency response [16, 17]. While the majority of our focus in this paper is on exterior problems, the techniques outlined here can also be applied for studying interior problems.

Traditionally, interior problems involving these boundary conditions have been treated using the finite element method (FEM) [18, 19, 20, 21]. For the clamped and supported plate problems, there are well-understood error estimates [22, 23] and software packages available for dealing with complex geometries. However, very few error estimates or high-order implementations exist for the free plate problem, which is typically solved on relatively simple geometries. FEM also makes it challenging to study exterior problems since it requires one to discretize the entire region containing both the scattering object and the points where one hopes to obtain the solution, while truncating the domain and solving auxiliary constraints at artificial boundaries. This is either done with transparent boundary conditions [24, 25] or perfectly matched layers [26], where it is difficult to achieve zero reflectance for complicated wave phenomena.

An alternative approach is to recast the PDE as an integral equation defined on the boundary of the domain. In general, this is possible whenever the PDE is linear and elliptic, with known Green's function [27]. The basic approach is to define the solution of the PDE in terms of a layer potential with an unknown density defined on the boundary of the domain.

The layer potential is designed to automatically satisfy the PDE within the domain, while the unknown density is determined by enforcing the boundary conditions on the boundary traces of the layer potential, resulting in a boundary integral equation (BIE).

Numerically, BIEs offer several advantages over direct discretization or weak formulation of the PDE. One feature of BIEs is that all of the unknowns are located on the boundary of the domain, and hence only the boundary needs to be discretized. This is particularly useful for solving exterior problems, where any necessary radiation conditions can be incorporated into the definition of the layer potential. There are further advantages for BIEs that are also second kind integral equations (SKIEs) in which the operator applied to the density is the sum of a bounded invertible operator and a compact operator. There is a well-established theory for analyzing the existence and uniqueness of solutions to SKIEs via the Fredholm alternative, as well as their behavior under discretization [28, 29, 30]. In particular, the condition number of the discretized SKIE system will remain bounded as the boundary mesh is refined.

There is a significant literature for BIEs in the biharmonic problem (k = 0), particularly for the clamped plate boundary conditions. SKIEs based on multiple-layer representations were historically applied to analyze the existence, uniqueness, and regularity of solutions of the clamped plate problem [31, 32]. An alternative route to the clamped plate problem can be pursued by converting the problem to a Stokes problem, for which there are particularly nice representations [33, 34]. A general approach for the k = 0 case with both clamped plate and free plate BCs is developed in [35, §2.4] by analogy with the second order case, though the resulting boundary operators are not exactly SKIEs but include hypersingular operators. It is also possible to solve the supported plate problem by reduction to a system of two Poisson equations [36, 37], but this method requires volume integration and has no clear extension to the case when $k \neq 0$.

The thesis [1] describes a different framework for developing layer potential representations. The basic idea is to select linear combinations of derivatives of the Green's function such that the resulting BIE is second kind and that the integral kernels in the BIE are as smooth as possible. In [1], the technique is applied to the k=0 case for the clamped plate, fluid mechanics (∇u is prescribed on the boundary), and supported plate BCs, though with limited success in the case of the fluid mechanics and supported plate BCs. In particular, the BIEs for the fluid mechanics and supported plate problems contain differential operators and therefore their condition number is unbounded. For the clamped plate problem, the framework of [1] extends readily to three dimensions [38] and to nonzero k [15].

In contrast with the steady-state (k=0) case, the oscillatory problem has received less attention, despite being a central focus of texts on structural engineering and elastic physics [4, 10]. Previous attempts have relied on factoring the solution into Helmholtz and modified Helmholtz equations and solving a coupled system at the boundary [24, 39, 40]. These combined BIEs can suffer from ill-conditioning though effective pre-conditioning strategies exist [39]. These approaches are currently not capable of solving the free or supported plate problems, which motivates the development of the present BIEs. Compared with previous methods, we gain degrees of freedom in the design of the integral representation by taking standard layer potentials and composing them with the Hilbert transform.

The remainder of the paper is as follows. In section 2, we give an overview of the Green's function and the boundary integral framework that will be used to solve this problem. In section 3, we review the kernels previously used by [1, 15] for solving the clamped plate problem and discuss their application to exterior problems. In section 4, we present a novel representation for the free plate problem which uses the Hilbert transform in the representation of the solution. In section 5, we give a representation for the supported plate which is similar to [1], but uses extra terms to ensure that the BIE is second kind. In section 6, we discuss details of the implementation of these methods used for the numerical results, describing a high-order-accurate approach to discretize the integral equations and stable methods to evaluate the kernels. In section 7, we present numerical results illustrating high-order convergence, and the application of these methods to solve scattering problems, including scattering from a large collection of objects. Finally, in section 8, we discuss the significance of the present work and the potential for using integral equations to model sea ice and ice shelves in the future.

2. Mathematical Framework and BIE Formalism

The Green's function for the free-space problem is defined as the solution to the equation

$$\Delta^2 u - k^4 u = \delta(\mathbf{x} - \mathbf{y}) \tag{2}$$

where $\mathbf{x}, \mathbf{y} \in \mathbb{R}^2$, supplemented with the following radiation condition at infinity:

$$\frac{\mathbf{x}}{|\mathbf{x}|} \cdot \nabla u - iku = o(1/\sqrt{|\mathbf{x}|}) . \tag{3}$$

The Green's function for this problem can be written explicitly as

$$G(\mathbf{x}, \mathbf{y}) = \frac{1}{2k^2} \left[\frac{i}{4} H_0^{(1)}(k|\mathbf{x} - \mathbf{y}|) - \frac{1}{2\pi} K_0(k|\mathbf{x} - \mathbf{y}|) \right]$$
(4)

where $H_0^{(1)}$ is the zero-th order Hankel function of the first kind and K_0 is the zero-th order modified Bessel function of the second kind. This Green's function is a scaled difference of the Green's functions for the Helmholtz and Yukawa equations, which oscillate and decay, respectively. As such, G automatically satisfies the natural radiation condition (3).

In the BIE framework, we seek to represent the solution to a boundary value problem (BVP) as a combination of integral operators applied to some densities on the boundary:

$$u(\mathbf{x}) = \mathcal{K}_1[\rho_1](\mathbf{x}) + \mathcal{K}_2[\rho_2](\mathbf{x})$$
(5)

where ρ_1 and ρ_2 are densities that lie in a suitable function space on the boundary (e.g. $L^2(\partial\Omega)$) and where the integral operators \mathcal{K}_1 and \mathcal{K}_2 are given by

$$\mathcal{K}_1[\rho_1](\mathbf{x}) := \int_{\partial\Omega} K_1(\mathbf{x}, \mathbf{y}) \rho_1(\mathbf{y}) \, \mathrm{d}S(\mathbf{y}) \tag{6}$$

$$\mathcal{K}_2[\rho_2](\mathbf{x}) := \int_{\partial\Omega} K_2(\mathbf{x}, \mathbf{y}) \rho_2(\mathbf{y}) \, \mathrm{d}S(\mathbf{y}) . \tag{7}$$

In this formalism, we represent the solution of the BVP using a collection of "charges" (sources, dipoles, and multipoles) defined on the boundary $\partial\Omega$. The kernels K_1 and K_2 typically involve derivatives of the Green's function, so that the representation automatically satisfies (1) in the interior. To ensure that this solution also satisfies the BCs, one must plug this representation into the boundary conditions and take the limit as the target approaches the boundary. This leads to a 2×2 system of integral equations on the boundary $\partial\Omega$:

$$\begin{pmatrix} D_{11} & D_{12} \\ D_{21} & D_{22} \end{pmatrix} \begin{pmatrix} \rho_1(\mathbf{x}) \\ \rho_2(\mathbf{x}) \end{pmatrix} + \text{p.v.} \int_{\partial \Omega} \begin{pmatrix} K_{11}(\mathbf{x}, \mathbf{y}) & K_{12}(\mathbf{x}, \mathbf{y}) \\ K_{21}(\mathbf{x}, \mathbf{y}) & K_{22}(\mathbf{x}, \mathbf{y}) \end{pmatrix} \begin{pmatrix} \rho_1(\mathbf{y}) \\ \rho_2(\mathbf{y}) \end{pmatrix} dS(\mathbf{y}) = \begin{pmatrix} f_1(\mathbf{x}) \\ f_2(\mathbf{x}) \end{pmatrix} , \quad (8)$$

where p.v. indicates that the (possibly singular) integral is to be understood in the principal value sense. It is useful to define the on-surface integral operators as well:

$$\mathcal{K}_{ij}[\rho_j](\mathbf{x}) := \text{p.v.} \int_{\partial\Omega} K_{ij}(\mathbf{x}, \mathbf{y}) \rho_j(\mathbf{y}) \, dS(\mathbf{y})$$
(9)

The jump matrix $\mathbf{D} := \begin{pmatrix} D_{11} & D_{12} \\ D_{21} & D_{22} \end{pmatrix}$ is often referred to as the constant or identity part of the integral equation and is precisely the difference between the limit of the integral operator as it approaches the boundary and the operator on the boundary:

$$D_{ij}\rho_j(\mathbf{x}_0) := \lim_{\mathbf{x} \to \mathbf{x}_0} \int_{\partial\Omega} K_{ij}(\mathbf{x}, \mathbf{y}) \rho_j(\mathbf{y}) \, \mathrm{d}S(\mathbf{y}) - \text{p.v.} \int_{\partial\Omega} K_{ij}(\mathbf{x}_0, \mathbf{y}) \rho_j(\mathbf{y}) \, \mathrm{d}S(\mathbf{y})$$
(10)

Meanwhile, the kernel matrix $\mathbf{K} := \begin{pmatrix} K_{11} & K_{12} \\ K_{21} & K_{22} \end{pmatrix}$ consists of the kernels K_1 and K_2 plugged into the corresponding boundary conditions. The expressions f_1 and f_2 on the right-hand side depend on the boundary data. When the jump matrix \mathbf{D} is bounded and invertible and the integral operators \mathcal{K}_{ij} are compact, the equation is referred to as a second kind integral equation (SKIE). The goal of this paper is to design kernels K_1 and K_2 for each of the clamped plate, free plate, and supported plate BCs so that system (8) is an SKIE.

In the remainder of the manuscript, we use the following conventions for notation. The boundary, $\partial\Omega$, is assumed to be a smooth curve. For a point \mathbf{x} on $\partial\Omega$, $n(\mathbf{x})$ is the outward-pointing normal, $\tau(\mathbf{x})$ is the positively-oriented (clockwise) unit tangent vector, and $\kappa(\mathbf{x})$ is the signed curvature at the point \mathbf{x} . The value s denotes arc-length along the curve. The input to the Green's function is usually of the form $G(\mathbf{x}, \mathbf{y})$, where \mathbf{x} is sometimes referred to as the "target" and \mathbf{y} as the "source." We often employ the more compact notation $n_{\mathbf{x}} = n(\mathbf{x})$, $\tau_{\mathbf{y}} = \tau(\mathbf{y})$, etc. We denote directional derivatives of the Green's function by subscripts, e.g. $G_{n_{\mathbf{x}}}(\mathbf{x}, \mathbf{y}) = n(\mathbf{x}) \cdot \nabla_{\mathbf{x}} G(\mathbf{x}, \mathbf{y})$ and $G_{\tau_{\mathbf{y}}} = \tau(\mathbf{y}) \cdot \nabla_{\mathbf{y}} G$. Multiple subscripts correspond to contractions of the Hessian or other higher-order derivative tensors of G with the indicated directions, e.g.

$$G_{n_{\mathbf{x}}\tau_{\mathbf{x}}\tau_{\mathbf{y}}}(\mathbf{x}, \mathbf{y}) = n_{\mathbf{x}} \cdot \nabla_{\mathbf{w}} \left(\tau_{\mathbf{x}} \cdot \nabla_{\mathbf{w}} \left(\tau_{\mathbf{y}} \cdot \nabla_{\mathbf{z}} G(\mathbf{w}, \mathbf{z}) \right) \right) |_{\mathbf{w} = \mathbf{x}, \mathbf{z} = \mathbf{y}}$$
(11)

An important distinction is that

$$\frac{\mathrm{d}}{\mathrm{d}s}G(\mathbf{x}(s),\mathbf{y}) = G_{\tau_{\mathbf{x}}}(\mathbf{x}(s),\mathbf{y}) \quad \text{but} \quad \frac{\mathrm{d}^{2}}{\mathrm{d}s^{2}}G(\mathbf{x}(s),\mathbf{y}) = G_{\tau_{\mathbf{x}}\tau_{\mathbf{x}}}(\mathbf{x}(s),\mathbf{y}) - \kappa(\mathbf{x}(s))G_{n_{\mathbf{x}}}(\mathbf{x}(s),\mathbf{y})$$
(12)

which can be easily seen through application of the product rule.

3. Clamped Plate Problem

First we consider the BVP with clamped plate BCs:

$$\begin{cases} u = f_1 & \text{on } \partial\Omega \\ \frac{\partial u}{\partial n} = f_2 & \text{on } \partial\Omega \end{cases}$$
 (13)

These BCs are commonly used in engineering when a planar material is welded to its frame along the perimeter, such as the hull of a ship [41] or an aircraft wing [42, 43]. Within geophysics, these boundary conditions are used to describe floating ice that is anchored along its edges, for instance an ice shelf that is permanently moored at its grounding line [44, 45]. When a plate is fixed at its boundary, it is unable to bend to absorb and release the energy of the wave. This creates a state of high internal stress near the grounding line of an ice shelf [46], making it a vulnerable and therefore important area to study [47].

As noted in the introduction, [1] developed kernels for the biharmonic equation (k = 0) by selecting linear combinations of derivatives of the Green's function to optimize the regularity of the resulting boundary integral equation kernels. These same linear combinations apply readily to the case of non-zero k [15]. For the sake of completeness, we reproduce these kernels here:

$$K_1 = G_{n_{\mathbf{v}}n_{\mathbf{v}}n_{\mathbf{v}}} + 3G_{n_{\mathbf{v}}\tau_{\mathbf{v}}\tau_{\mathbf{v}}} \tag{14}$$

$$K_2 = -G_{n_{\mathbf{y}}n_{\mathbf{y}}} + G_{\tau_{\mathbf{y}}\tau_{\mathbf{y}}} \tag{15}$$

This choice of kernels results in the following identity part of the integral equation for the exterior problem:

$$\mathbf{D}_{\text{ext}} = \begin{pmatrix} -\frac{1}{2} & 0\\ \kappa(\mathbf{x}) & -\frac{1}{2} \end{pmatrix}, \ \mathbf{x} \in \partial\Omega$$
 (16)

where $\kappa(\mathbf{x})$ is the signed curvature of the boundary. For the interior problem, the same choice of kernels results in the following identity since the limit is taken from the inside rather than the outside:

$$\mathbf{D}_{\text{int}} = \begin{pmatrix} \frac{1}{2} & 0\\ -\kappa(\mathbf{x}) & \frac{1}{2} \end{pmatrix}, \ \mathbf{x} \in \partial\Omega$$
 (17)

Below are the kernels which appear in the integral equation:

$$K_{11} = G_{n_{\mathbf{v}}n_{\mathbf{v}}n_{\mathbf{v}}} + 3G_{n_{\mathbf{v}}\tau_{\mathbf{v}}\tau_{\mathbf{v}}} \tag{18}$$

$$K_{12} = -G_{n_{\mathbf{v}}n_{\mathbf{v}}} + G_{\tau_{\mathbf{v}}\tau_{\mathbf{v}}} \tag{19}$$

$$K_{21} = G_{n_{\mathbf{x}}n_{\mathbf{y}}n_{\mathbf{y}}n_{\mathbf{y}}} + 3G_{n_{\mathbf{x}}n_{\mathbf{y}}\tau_{\mathbf{y}}\tau_{\mathbf{y}}}$$

$$\tag{20}$$

$$K_{22} = -G_{n_{\mathbf{x}}n_{\mathbf{y}}n_{\mathbf{y}}} + G_{n_{\mathbf{x}}\tau_{\mathbf{y}}\tau_{\mathbf{y}}} \tag{21}$$

Lemma 1. The layer potentials of the flexural wave equation satisfy the exact same jump relations as those of the biharmonic equation introduced in [1].

Proof. We employ the same argument as in [15] with the flexural wave Green's function $G(\mathbf{x}, \mathbf{y}) := \frac{1}{2k^2} \left[\frac{i}{4} H_0^{(1)}(k|\mathbf{x} - \mathbf{y}|) - \frac{1}{2\pi} K_0(k|\mathbf{x} - \mathbf{y}|) \right]$. Using the power series formulae for the Bessel functions J_0 and Y_0 [48, §10.8], we have that

$$H_0^{(1)}(k|\mathbf{x} - \mathbf{y}|) = \Psi_k(\mathbf{x}, \mathbf{y}) + \frac{2i}{\pi} \ln|\mathbf{x} - \mathbf{y}| \sum_{m>0} \frac{(-1)^m}{(m!)^2} \left(\frac{k|\mathbf{x} - \mathbf{y}|}{2}\right)^{2m}, \qquad (22)$$

where $\Psi_k(\mathbf{x}, \mathbf{y})$ is a smooth function. Likewise,

$$K_0(k|\mathbf{x} - \mathbf{y}|) = \frac{\pi i}{2} \Psi_{ik}(\mathbf{x}, \mathbf{y}) - \ln|\mathbf{x} - \mathbf{y}| \sum_{m>0} \frac{1}{(m!)^2} \left(\frac{k|\mathbf{x} - \mathbf{y}|}{2}\right)^{2m}.$$
 (23)

Combining these, we obtain

$$G(\mathbf{x}, \mathbf{y}) = \Phi_k(\mathbf{x}, \mathbf{y}) + \frac{1}{4\pi k^2} \ln|\mathbf{x} - \mathbf{y}| \sum_{m>0} \frac{1 - (-1)^m}{(m!)^2} \left(\frac{k|\mathbf{x} - \mathbf{y}|}{2}\right)^{2m},$$
(24)

where $\Phi_k(\mathbf{x}, \mathbf{y}) = \frac{i}{8k^2}(\Psi_k(\mathbf{x}, \mathbf{y}) - \Psi_{ik}(\mathbf{x}, \mathbf{y}))$ is a smooth function. Separating out the first non-zero term from the sum, we have

$$G(\mathbf{x}, \mathbf{y}) = \Phi_k(\mathbf{x}, \mathbf{y}) + \frac{1}{8\pi} |\mathbf{x} - \mathbf{y}|^2 \ln|\mathbf{x} - \mathbf{y}| + \frac{1}{4\pi k^2} \ln|\mathbf{x} - \mathbf{y}| \sum_{m \ge 3} \frac{1 - (-1)^m}{(m!)^2} \left(\frac{k|\mathbf{x} - \mathbf{y}|}{2}\right)^{2m},$$
(25)

so that the leading non-smooth term is precisely the Green's function of the biharmonic equation. Additionally, the next order term takes the form $|\mathbf{x} - \mathbf{y}|^6 \ln(|\mathbf{x} - \mathbf{y}|)$. Since our kernels have at most four derivatives of the Green's function, we conclude that the jump relations should be the same as those computed in [1].

Theorem 1. The kernel functions K_{11} , K_{12} , K_{21} , and K_{22} are continuous.

Proof. Let $G(\mathbf{x}, \mathbf{y}) = \frac{1}{2k^2} (\frac{i}{4} H_0^{(1)}(k|\mathbf{x} - \mathbf{y}|) - \frac{1}{2\pi} K_0(k|\mathbf{x} - \mathbf{y}|))$. It is sufficient for us to show the continuity of the kernel functions as $|\mathbf{x} - \mathbf{y}| \to 0$. Based on the asymptotic expansion derived above, we only need to analyze the smoothness of the corresponding derivatives of $G^B = \frac{1}{8\pi} |\mathbf{x} - \mathbf{y}|^2 \ln |\mathbf{x} - \mathbf{y}|$. Since $\partial \Omega$ is smooth, the functions

$$K_{11}^B = G_{n_{\mathbf{y}}n_{\mathbf{y}}n_{\mathbf{y}}}^B + 3G_{n_{\mathbf{y}}\tau_{\mathbf{y}}\tau_{\mathbf{y}}}^B \tag{26}$$

$$K_{12}^B = -G_{n_{\mathbf{v}}n_{\mathbf{v}}}^B + G_{\tau_{\mathbf{v}}\tau_{\mathbf{v}}}^B \tag{27}$$

$$K_{21}^B = G_{n_{\mathbf{x}}n_{\mathbf{y}}n_{\mathbf{y}}n_{\mathbf{y}}}^B + 3G_{n_{\mathbf{x}}n_{\mathbf{y}}\tau_{\mathbf{y}}\tau_{\mathbf{y}}}^B \tag{28}$$

$$K_{22}^B = -G_{n_{\mathbf{x}}n_{\mathbf{y}}n_{\mathbf{y}}}^B + G_{n_{\mathbf{x}}\tau_{\mathbf{y}}\tau_{\mathbf{y}}}^B \tag{29}$$

are smooth by [1]. Thus, we conclude that K_{11} , K_{12} , K_{21} , and K_{22} are continuous.

Corollary 1. The integral equation associated to (16)-(21) is Fredholm second kind.

4. Free Plate Problem

Next we turn our attention to the free plate problem. The boundary conditions for an arbitrary curve with arclength parameterization $\gamma(s)$ is given by:

$$\begin{cases} \nu \Delta u + (1 - \nu) \frac{\partial^2 u}{\partial n^2} = f_1 & \text{on } \partial \Omega \\ \frac{\partial \Delta u}{\partial n} + (1 - \nu) \frac{\mathrm{d}}{\mathrm{d}s} \frac{\partial^2 u}{\partial n \partial \tau} = f_2 & \text{on } \partial \Omega \end{cases}$$
(30)

The first equation corresponds to a prescribed bending moment, while the second equation corresponds to the Kirchhoff equivalent shear force [2]. While the clamped plate fixes the displacement and leaves forces as unknowns, the free edge represents the opposite scenario, where the forces are prescribed on the boundary and the displacement is unknown. To accommodate these forces, the plate is allowed to oscillate freely at its boundary, leading to edge waves with interesting dynamics [49]. Within the realm of geophysics, these boundary conditions are used to model the edges of ice shelves and ice floes which are floating freely atop the ocean [44, 50, 21]. In this case, it is typical to set both conditions to zero and allow wave coupling to occur through the underlying medium.

Using the Frenet-Serret identities $\frac{d\tau}{ds} = -\kappa n$ and $\frac{dn}{ds} = \kappa \tau$, the second condition in (30) can be re-written as:

$$\frac{\partial^3 u}{\partial n^3} + (2 - \nu) \frac{\partial^3 u}{\partial n \partial \tau^2} + (1 - \nu) \kappa \left(\frac{\partial^2 u}{\partial \tau^2} - \frac{\partial^2 u}{\partial n^2} \right) = f_2 \quad \text{on } \partial\Omega$$
 (31)

Before proceeding, we recall the definitions of several integral operators: the Hilbert transform, Laplace double layer, and normal and tangential derivatives of the Laplace single layer for an arbitrary curve $\partial\Omega$. In the section that follows, integral operators are denoted using calligraphic letters while the kernels of those integral operators are denoted using capital letters.

Definition 1. The Hilbert transform \mathcal{H} of a function f on $\partial\Omega$ is given by:

$$\mathcal{H}[f](\mathbf{x}) = \int_{\partial\Omega} \frac{1}{\pi} \frac{(\mathbf{x} - \mathbf{y}) \cdot \tau(\mathbf{y})}{|\mathbf{x} - \mathbf{y}|^2} f(\mathbf{y}) \, \mathrm{d}S(\mathbf{y})$$
(32)

Definition 2. The Laplace double layer potential \mathcal{D} of a function f on $\partial\Omega$ is given by:

$$\mathcal{D}[f](\mathbf{x}) = \frac{1}{2\pi} \int_{\partial \Omega} \frac{(\mathbf{x} - \mathbf{y}) \cdot n(\mathbf{y})}{|\mathbf{x} - \mathbf{y}|^2} f(\mathbf{y}) \, dS(\mathbf{y})$$
(33)

Definition 3. The tangential derivative of the Laplace single layer S of a function f on $\partial\Omega$ is given by:

$$S_{\tau}[f](\mathbf{x}) = \frac{1}{2\pi} \int_{\partial\Omega} \frac{(\mathbf{x} - \mathbf{y}) \cdot \tau(\mathbf{x})}{|\mathbf{x} - \mathbf{y}|^2} f(\mathbf{y}) \, \mathrm{d}S(\mathbf{y})$$
(34)

Definition 4. The normal derivative of the Laplace single layer S of a function f on $\partial\Omega$ is given by:

$$S'[f](\mathbf{x}) = \frac{1}{2\pi} \int_{\partial\Omega} \frac{(\mathbf{x} - \mathbf{y}) \cdot n(\mathbf{x})}{|\mathbf{x} - \mathbf{y}|^2} f(\mathbf{y}) \, dS(\mathbf{y})$$
(35)

This leads us to the following statement which is a special case of the Poincaré-Bertrand formula; see, for example, [51, 52] and the references therein.

Remark 1. Given the Laplace single layer potential S of a function f defined on a smooth curve $\partial\Omega$, we have the following identity regarding the composition of single layer potentials:

$$S_{\tau}^2 = -\frac{I}{4} + S^2 \tag{36}$$

The following consequence will be heavily relied on in the derivation of the free plate integral equation:

Remark 2. Taking the adjoint of (36), we have the following relationship regarding the composition of the Hilbert transform with itself for an arbitrary curve:

$$\frac{1}{4}\mathcal{H}^2 = -\frac{I}{4} + \mathcal{D}^2 \tag{37}$$

With this statement in mind, we write the representation of the solution to (30) as:

$$\mathcal{K}_1 = \mathcal{K}_1^a + \mathcal{K}_1^b \mathcal{H} \tag{38}$$

$$\mathcal{K}_2 = \mathcal{K}_2 \tag{39}$$

where the kernels of these integral operators are given by:

$$K_1^a = G_{n_{\mathbf{v}}} \tag{40}$$

$$K_1^b = \beta G_{\tau_{\mathbf{y}}} \tag{41}$$

$$K_2 = G (42)$$

where $\beta = \frac{1+\nu}{2}$ and \mathcal{H} is the Hilbert transform defined above. The corresponding identity matrix for the integral equation is:

$$\mathbf{D}_{\text{ext}} = \begin{pmatrix} -\frac{1}{2} + \frac{\beta^2}{2} & 0\\ 0 & \frac{1}{2} \end{pmatrix}$$
 (43)

Using the identities in section three, the corresponding integral operators in the integral equation for the exterior problem are:

$$\mathcal{K}_{11} = \mathcal{M}_1 + \beta \mathcal{M}_2 \mathcal{H} - 2\beta^2 \mathcal{D}^2 \tag{44}$$

$$\mathcal{K}_{12} = \mathcal{M}_3 \tag{45}$$

$$\mathcal{K}_{21} = \mathcal{M}_4 + \beta \mathcal{M}_5 \mathcal{H} + (1 - \nu) \kappa(\mathbf{x}) \left(\mathcal{M}_6 + \beta \mathcal{M}_7 \mathcal{H} \right) \tag{46}$$

$$\mathcal{K}_{22} = \mathcal{M}_8 + (1 - \nu)\kappa(\mathbf{x})\mathcal{M}_9 \tag{47}$$

where $\mathbf{x} \in \partial \Omega$ and \mathcal{D} is the Laplace double layer given in (33). The kernels M_n (n = 1, 2, ..., 9) of the integral operators \mathcal{M}_n above are given by

$$M_1 = G_{n_{\mathbf{x}}n_{\mathbf{y}}n_{\mathbf{y}}} + \nu G_{\tau_{\mathbf{x}}\tau_{\mathbf{x}}n_{\mathbf{y}}} \tag{48}$$

$$M_2 = G_{n_{\mathbf{x}}n_{\mathbf{x}}\tau_{\mathbf{y}}} + \frac{1}{4}K^{\mathcal{H}ilb} + \nu(G_{\tau_{\mathbf{x}}\tau_{\mathbf{x}}\tau_{\mathbf{y}}} + \frac{1}{4}K^{\mathcal{H}ilb})$$

$$\tag{49}$$

$$M_3 = G_{n_{\mathbf{x}}n_{\mathbf{x}}} + \nu G_{\tau_{\mathbf{x}}\tau_{\mathbf{x}}} \tag{50}$$

$$M_4 = G_{n_{\mathbf{x}}n_{\mathbf{x}}n_{\mathbf{y}}} + (2 - \nu)G_{n_{\mathbf{x}}\tau_{\mathbf{x}}\tau_{\mathbf{y}}n_{\mathbf{y}}} - \frac{\beta}{2} \frac{\mathrm{d}}{\mathrm{d}s} K^{\mathcal{H}ilb}$$
(51)

$$M_5 = G_{n_{\mathbf{x}}n_{\mathbf{x}}n_{\mathbf{x}}\tau_{\mathbf{y}}} + (2 - \nu)G_{n_{\mathbf{x}}\tau_{\mathbf{x}}\tau_{\mathbf{x}}\tau_{\mathbf{y}}}$$

$$\tag{52}$$

$$M_6 = G_{\tau_{\mathbf{x}}\tau_{\mathbf{x}}n_{\mathbf{y}}} - G_{n_{\mathbf{x}}n_{\mathbf{x}}n_{\mathbf{y}}} \tag{53}$$

$$M_7 = \left(G_{\tau_{\mathbf{x}}\tau_{\mathbf{x}}\tau_{\mathbf{y}}} + \frac{1}{4}K^{\mathcal{H}ilb}\right) - \left(G_{n_{\mathbf{x}}n_{\mathbf{x}}\tau_{\mathbf{y}}} + \frac{1}{4}K^{\mathcal{H}ilb}\right) \tag{54}$$

$$M_8 = G_{n_{\mathbf{x}}n_{\mathbf{x}}n_{\mathbf{x}}} + (2 - \nu)G_{n_{\mathbf{x}}\tau_{\mathbf{x}}\tau_{\mathbf{x}}}$$

$$\tag{55}$$

$$M_9 = G_{\tau_{\mathbf{x}}\tau_{\mathbf{x}}} - G_{n_{\mathbf{x}}n_{\mathbf{x}}} \tag{56}$$

where $K^{\mathcal{H}ilb}$ is the kernel of the Hilbert transform (32) and $\frac{\mathrm{d}}{\mathrm{d}s}$ is the arclength derivative taken with respect to the target variable \mathbf{x} .

Theorem 2. The functions M_n are continuous for $n \neq 3$ and weakly (log) singular for n = 3.

Proof. Let $G(\mathbf{x}, \mathbf{y}) = \frac{1}{2k^2} (\frac{i}{4} H_0^{(1)}(k|\mathbf{x} - \mathbf{y}|) - \frac{1}{2\pi} K_0(k|\mathbf{x} - \mathbf{y}|))$ and $G^B(\mathbf{x}, \mathbf{y}) = \frac{1}{8\pi} \ln(|\mathbf{x} - \mathbf{y}|)|\mathbf{x} - \mathbf{y}|^2$ for $\mathbf{x}, \mathbf{y} \in \partial \Omega$. As before, it's sufficient for us to show the continuity of these functions as $|\mathbf{x} - \mathbf{y}| \to 0$ and analyze the functions M_n^B (n = 1, ..., 9), which is defined by applying the same derivatives to G^B . Suppose $\gamma(t)$ is the arc-length parametrization to the boundary $\partial \Omega$. By Taylor expansion, we can have:

$$\gamma(t+s) - \gamma(t) = s\tau(t) - \frac{s^{2}}{2}\kappa(t)n(t) - \frac{s^{3}}{6}(\kappa'(t)n(t) + \kappa^{2}(t)\tau(t)) + \frac{s^{4}}{24}((-\kappa''(t) + \kappa^{3}(t))n(t) - 3\kappa(t)\kappa'(t)\tau(t)) + \mathcal{O}(s^{5})$$
(57)

where $\kappa(t)$ is the curvature of $\partial\Omega$ at t and $\kappa'(t)$ is the arc length derivative of curvature at t. Without loss of generality, set t=0 and let $\mathbf{x}=\boldsymbol{\gamma}(0)=0$ and $\mathbf{y}=\boldsymbol{\gamma}(s)$ for $\mathbf{x},\mathbf{y}\in\partial\Omega$. Expanding \mathbf{y} about 0 we get:

$$\mathbf{y} = s\tau(0) - \frac{s^2}{2}\kappa(0)n(0) - \frac{s^3}{6}(\kappa'(0)n(0) + \kappa^2(0)\tau(0))$$

$$+\frac{s^4}{24}((-\kappa''(0)+\kappa^3(0))n(0)-3\kappa(0)\kappa'(0)\tau(0))+\mathcal{O}(s^5) \quad (58)$$

Similarly, we can expand $\tau(\mathbf{y})$ and $n(\mathbf{y})$ as:

$$\tau(\mathbf{y}) = \tau(0) - s\kappa(0)n(0) - \frac{s^2}{2}(\kappa'(0)n(0) + \kappa^2(0)\tau(0)) + \frac{s^3}{6}((-\kappa''(0) + \kappa^3(0))n(0) - 3\kappa(0)\kappa'(0)\tau(0)) + \mathcal{O}(s^4)$$
(59)
$$n(\mathbf{y}) = n(0) + s\kappa(0)\tau(0) + \frac{s^2}{2}(\kappa'(0)\tau(0) - \kappa^2(0)n(0)) + \frac{s^3}{6}((\kappa''(0) - \kappa^3(0))\tau(0) - 3\kappa(0)\kappa'(0)n(0)) + \mathcal{O}(s^4)$$
(60)

Using these expansions, we first look at $M_1^B = G_{n_{\mathbf{x}}n_{\mathbf{x}}n_{\mathbf{y}}}^B + \nu G_{\tau_{\mathbf{x}}\tau_{\mathbf{x}}n_{\mathbf{y}}}^B$. The closed form formulae for $G_{n_{\mathbf{x}}n_{\mathbf{x}}n_{\mathbf{y}}}^B$ and $G_{\tau_{\mathbf{x}}\tau_{\mathbf{x}}n_{\mathbf{y}}}^B$ are in Appendix B.2. Direct substitution gives:

$$G_{n_{\mathbf{x}}n_{\mathbf{x}}n_{\mathbf{y}}}^{B}(\mathbf{x}, \mathbf{y}) = -\frac{1}{8\pi}\kappa(0) + \mathcal{O}(s)$$
(61)

$$G_{\tau_{\mathbf{x}}\tau_{\mathbf{x}}n_{\mathbf{y}}}^{B}(\mathbf{x}, \mathbf{y}) = \frac{3}{8\pi}\kappa(0) + \mathcal{O}(s)$$
(62)

Taking the limits of $M_1^B(\mathbf{x}, \mathbf{y})$ and $M_6^B(\mathbf{x}, \mathbf{y})$ as the source approaches the target, we get:

$$\lim_{s \to 0} M_1^B(\mathbf{x}, \mathbf{y}) = \frac{3\nu - 1}{8\pi} \kappa(\mathbf{x})$$
(63)

$$\lim_{s \to 0} M_6^B(\mathbf{x}, \mathbf{y}) = \frac{1}{2\pi} \kappa(\mathbf{x})$$
 (64)

For a smooth curve, these limits are well defined, so we conclude that M_1^B is continuous. Repeating this calculation for terms in M_8^B , we have:

$$G_{n_{\mathbf{x}}n_{\mathbf{x}}n_{\mathbf{x}}}^{B}(\mathbf{x}, \mathbf{y}) = \frac{3}{8\pi}\kappa(0) + \mathcal{O}(s)$$
(65)

$$G_{n_{\mathbf{x}}\tau_{\mathbf{x}}\tau_{\mathbf{x}}}^{B}(\mathbf{x}, \mathbf{y}) = -\frac{1}{8\pi}\kappa(0) + \mathcal{O}(s)$$
(66)

Taking the limit of $M_8^B(\mathbf{x}, \mathbf{y})$ as the source approaches the target, we get:

$$\lim_{\mathbf{x} \to 0} M_8^B(\mathbf{x}, \mathbf{y}) = \frac{1 + \nu}{8\pi} \kappa(\mathbf{x})$$
 (67)

We now analyze $M_2^B = G_{n_{\mathbf{x}}n_{\mathbf{x}}\tau_{\mathbf{y}}}^B + \frac{1}{4}K^{\mathcal{H}ilb} + \nu(G_{\tau_{\mathbf{x}}\tau_{\mathbf{x}}\tau_{\mathbf{y}}}^B + \frac{1}{4}K^{\mathcal{H}ilb})$. Substituting the above Taylor expansions into the closed form formulas of $G_{n_{\mathbf{x}}n_{\mathbf{x}}\tau_{\mathbf{y}}}^B$, $G_{\tau_{\mathbf{x}}\tau_{\mathbf{x}}\tau_{\mathbf{y}}}^B$ and $G_{r_{\mathbf{x}}r_{\mathbf{x}}\tau_{\mathbf{y}}}^B$, we obtain:

$$G_{n_{\mathbf{x}}n_{\mathbf{x}}\tau_{\mathbf{y}}}^{B}(\mathbf{x}, \mathbf{y}) = \frac{1}{4\pi} \frac{1}{s} + \mathcal{O}(s)$$
(68)

$$G_{\tau_{\mathbf{x}}\tau_{\mathbf{x}}\tau_{\mathbf{y}}}^{B}(\mathbf{x}, \mathbf{y}) = \frac{1}{4\pi} \frac{1}{s} + \mathcal{O}(s)$$
(69)

$$K^{\mathcal{H}ilb}(\mathbf{x}, \mathbf{y}) = -\frac{1}{\pi} \frac{1}{s} + \mathcal{O}(s)$$
 (70)

which gives:

$$\lim_{s \to 0} M_2^B(\mathbf{x}, \mathbf{y}) = 0 \tag{71}$$

Therefore M_2^B is continuous. From this calculation it is also clear that M_7^B is continuous. We now look at $M_4^B = G_{n_{\mathbf{x}}n_{\mathbf{x}}n_{\mathbf{y}}}^B + (2-\nu)G_{n_{\mathbf{x}}\tau_{\mathbf{x}}\tau_{\mathbf{x}}n_{\mathbf{y}}}^B - \frac{\beta}{2}\frac{\mathrm{d}}{\mathrm{d}s}K^{\mathcal{H}ilb}$. The closed form formula for $\frac{\mathrm{d}}{\mathrm{d}s}K^{\mathcal{H}ilb}$ is:

$$\frac{\mathrm{d}}{\mathrm{d}s}K^{\mathcal{H}ilb}(\mathbf{x},\mathbf{y}) = \frac{1}{\pi} \left(\frac{\tau(\mathbf{y}) \cdot \tau(\mathbf{x})}{|\mathbf{x} - \mathbf{y}|^2} - \frac{2[(\mathbf{x} - \mathbf{y}) \cdot \tau(\mathbf{x})][(\mathbf{x} - \mathbf{y}) \cdot \tau(\mathbf{y})]}{|\mathbf{x} - \mathbf{y}|^4} \right)$$
(72)

As before, let's substitute the Taylor expansions into the formulas of $G_{n_{\mathbf{x}}n_{\mathbf{x}}n_{\mathbf{x}}n_{\mathbf{y}}}^{B}$, $G_{n_{\mathbf{x}}\tau_{\mathbf{x}}\tau_{\mathbf{x}}n_{\mathbf{y}}}^{B}$, and $\frac{\mathrm{d}}{\mathrm{d}s}K^{\mathcal{H}ilb}$, which yields:

$$G_{n_{\mathbf{x}}n_{\mathbf{x}}n_{\mathbf{y}}}^{B}(\mathbf{x}, \mathbf{y}) = -\frac{3}{4\pi} \frac{1}{s^{2}} + \frac{5}{16\pi} \kappa^{2}(0) + \mathcal{O}(s)$$

$$(73)$$

$$G_{n_{\mathbf{x}}\tau_{\mathbf{x}}n_{\mathbf{y}}}^{B}(\mathbf{x}, \mathbf{y}) = \frac{1}{4\pi} \frac{1}{s^{2}} - \frac{17}{48\pi} \kappa^{2}(0) + \mathcal{O}(s)$$

$$(74)$$

$$\frac{\mathrm{d}}{\mathrm{d}s}K^{\mathcal{H}ilb}(\mathbf{x},\mathbf{y}) = -\frac{1}{\pi}\frac{1}{s^2} - \frac{1}{12\pi}\kappa^2(0) + \mathcal{O}(s)$$
(75)

which agrees with the arclength derivative of (70). Plugging these formulas into M_4 and taking the limit we get:

$$\lim_{s \to 0} M_4^B(\mathbf{x}, \mathbf{y}) = \frac{3(-1+\nu)}{8\pi} \kappa^2(\mathbf{x})$$
(76)

Therefore, since $\partial\Omega$ is smooth, we conclude that M_4^B is indeed continuous. Now, we analyze $M_5^B = G_{n_{\mathbf{x}}n_{\mathbf{x}}n_{\mathbf{x}}\tau_{\mathbf{y}}}^B + (2-\nu)G_{\tau_{\mathbf{x}}\tau_{\mathbf{x}}\tau_{\mathbf{y}}n_{\mathbf{x}}}^B$. Substituting the Taylor expansions into the closed-form formulas for $G_{n_{\mathbf{x}}n_{\mathbf{x}}n_{\mathbf{x}}\tau_{\mathbf{y}}}^B$ and $G_{\tau_{\mathbf{x}}\tau_{\mathbf{x}}\tau_{\mathbf{y}}n_{\mathbf{x}}}^B$, we get:

$$G_{n_{\mathbf{x}}n_{\mathbf{x}}\tau_{\mathbf{y}}}^{B}(\mathbf{x}, \mathbf{y}) = \frac{1}{8\pi}\kappa'(0) + \mathcal{O}(s)$$
(77)

$$G_{n_{\mathbf{x}}\tau_{\mathbf{x}}\tau_{\mathbf{y}}}^{B}(\mathbf{x}, \mathbf{y}) = -\frac{1}{24\pi}\kappa'(0) + \mathcal{O}(s)$$
(78)

which gives:

$$\lim_{s \to 0} M_5^B(\mathbf{x}, \mathbf{y}) = \frac{1 + \nu}{24\pi} \kappa'(\mathbf{x})$$
(79)

Since $\partial\Omega$ is smooth, we conclude that M_B^5 is also continuous. Finally, we look at $M_9^B=G_{\tau_{\mathbf{x}}\tau_{\mathbf{x}}}^B-G_{n_{\mathbf{x}}n_{\mathbf{x}}}^B$. Direct computation gives the closed-form formula:

$$M_9^B(\mathbf{x}, \mathbf{y}) = \frac{1}{4\pi} \frac{[(\mathbf{x} - \mathbf{y}) \cdot \tau(\mathbf{x})]^2 - [(\mathbf{x} - \mathbf{y}) \cdot n(\mathbf{x})]^2}{|\mathbf{x} - \mathbf{y}|^2} = \frac{1}{4\pi} - \frac{1}{2\pi} \frac{[(\mathbf{x} - \mathbf{y}) \cdot n(\mathbf{x})]^2}{|\mathbf{x} - \mathbf{y}|^2}$$
(80)

We use the Taylor expansions to find that the second term is $\mathcal{O}(s^2)$. Therefore:

$$\lim_{s \to 0} M_9^B(\mathbf{x}, \mathbf{y}) = \frac{1}{4\pi} \tag{81}$$

This concludes the proof that kernels (48)-(56) are continuous.

Corollary 2. The integral equation associated with (43)-(47) is Fredholm second kind.

Proof. It is sufficient for us to show that the integral operators \mathcal{K}_{11} , \mathcal{K}_{12} , \mathcal{K}_{21} , \mathcal{K}_{22} are compact. It is known from the theory of integral equations [28] that integral operators with continuous kernels on bounded domains are compact, so \mathcal{M}_n are compact for $n \neq 3$. It is also well-known that the Hilbert transform is a bounded operator, and a bounded operator composed with a compact operator is compact. Thus we conclude that $\mathcal{M}_2\mathcal{H}$, $\mathcal{M}_5\mathcal{H}$, and $\mathcal{M}_7\mathcal{H}$ are compact, which proves the compactness of \mathcal{K}_{11} , \mathcal{K}_{21} , and \mathcal{K}_{22} . Finally, we know that $\mathcal{M}_3(\mathbf{x}, \mathbf{y})$ has a logarithmic singularity. Thus, by results in [28], we know that $\mathcal{M}_3(\mathbf{x}, \mathbf{y})$ is weakly singular, hence giving the compactness of \mathcal{K}_{12} .

For the interior problem, we need to modify our choice of K_1 within the representation, since the limits are now taken from the interior rather than the exterior. Using the same notation, we choose the kernels in the representation to be:

$$K_1^a = -G_{n_n} \tag{82}$$

$$K_1^b = \beta G_{\tau_v} \tag{83}$$

$$K_2 = G (84)$$

This change leads to the following identity matrix:

$$\mathbf{D}_{\text{int}} = \begin{pmatrix} -\frac{1}{2} + \frac{\beta^2}{2} & 0\\ 0 & -\frac{1}{2} \end{pmatrix} \tag{85}$$

The corresponding kernel functions in the integral equation are:

$$\mathcal{K}_{11} = \mathcal{M}_1 + \beta \mathcal{M}_2 \mathcal{H} - 2\beta^2 \mathcal{D}^2 \tag{86}$$

$$\mathcal{K}_{12} = \mathcal{M}_3 \tag{87}$$

$$\mathcal{K}_{21} = \mathcal{M}_4 + \beta \mathcal{M}_5 \mathcal{H} + (1 - \nu) \kappa \left(\mathcal{M}_6 + \beta \mathcal{M}_7 \mathcal{H} \right)$$
 (88)

$$\mathcal{K}_{22} = \mathcal{M}_8 + (1 - \nu)\kappa \mathcal{M}_9 \tag{89}$$

where the kernels M_n (n = 1, ..., 9) of the integral operators above are:

$$M_1 = -(G_{n_{\mathbf{x}}n_{\mathbf{x}}n_{\mathbf{y}}} + \nu G_{\tau_{\mathbf{x}}\tau_{\mathbf{x}}n_{\mathbf{y}}}) \tag{90}$$

$$M_2 = G_{n_{\mathbf{x}}n_{\mathbf{x}}\tau_{\mathbf{y}}} + \frac{1}{4}K^{\mathcal{H}ilb} + \nu(G_{\tau_{\mathbf{x}}\tau_{\mathbf{x}}\tau_{\mathbf{y}}} + \frac{1}{4}K^{\mathcal{H}ilb})$$

$$\tag{91}$$

$$M_3 = G_{n_{\mathbf{x}}n_{\mathbf{x}}} + \nu G_{\tau_{\mathbf{x}}\tau_{\mathbf{x}}} \tag{92}$$

$$M_4 = -(G_{n_{\mathbf{x}}n_{\mathbf{x}}n_{\mathbf{x}}n_{\mathbf{y}}} + (2 - \nu)G_{n_{\mathbf{x}}\tau_{\mathbf{x}}\tau_{\mathbf{x}}n_{\mathbf{y}}}) + \frac{\beta}{2} \frac{\mathrm{d}}{\mathrm{d}s} K^{\mathcal{H}ilb}$$
(93)

$$M_5 = G_{n_{\mathbf{x}}n_{\mathbf{x}}n_{\mathbf{x}}\tau_{\mathbf{y}}} + (2 - \nu)G_{\tau_{\mathbf{x}}\tau_{\mathbf{x}}\tau_{\mathbf{y}}n_{\mathbf{x}}}$$

$$\tag{94}$$

$$M_6 = G_{n_{\mathbf{x}}n_{\mathbf{x}}n_{\mathbf{y}}} - G_{\tau_{\mathbf{x}}\tau_{\mathbf{x}}n_{\mathbf{y}}} \tag{95}$$

$$M_7 = \left(G_{\tau_{\mathbf{x}}\tau_{\mathbf{x}}\tau_{\mathbf{y}}} + \frac{1}{4}K^{\mathcal{H}ilb}\right) - \left(G_{n_{\mathbf{x}}n_{\mathbf{x}}\tau_{\mathbf{y}}} + \frac{1}{4}K^{\mathcal{H}ilb}\right) \tag{96}$$

$$M_8 = G_{n_{\mathbf{x}}n_{\mathbf{x}}n_{\mathbf{x}}} + (2 - \nu)G_{\tau_{\mathbf{x}}\tau_{\mathbf{x}}n_{\mathbf{x}}}$$

$$\tag{97}$$

$$M_9 = G_{\tau_{\mathbf{x}}\tau_{\mathbf{x}}} - G_{n_{\mathbf{x}}n_{\mathbf{x}}} \tag{98}$$

Repeating the same argument in Theorem 2 and Corollary 2, we know that the integral equation for the interior problem is Fredholm second kind.

5. Supported Plate Problem

In this section we will provide a boundary integral formulation for the supported plate, also referred to as the hinged plate. The boundary conditions for an arbitrary curve $\partial\Omega$ are:

$$u = f_1 \qquad \text{on } \partial\Omega$$
 (99)

$$\nu \Delta u + (1 - \nu) \frac{\partial^2 u}{\partial n^2} = f_2 \qquad \text{on } \partial \Omega$$
 (100)

As before, the first equation corresponds to fixed displacement while the second equation corresponds a prescribed bending moment. This occurs when a plate rests on a fixed support, but is not clamped to it, allowing the slope and shear force to vary at the boundary. These boundary conditions are used in many engineering applications to model the vibration of column supported slabs or circuit boards which are held up by internal supports [11, 53]. In glaciology, these boundary conditions are often used to model an ice shelf resting on a foundation of soft glacial till [54] or on a sloping seabed [55, 56].

For this problem we use a representation that is similar to [1] with the addition of a few terms that ensure compactness:

$$K_1 = G_{n_{\mathbf{y}}n_{\mathbf{y}}n_{\mathbf{y}}} + \alpha_1 G_{n_{\mathbf{y}}\tau_{\mathbf{y}}\tau_{\mathbf{y}}} + \alpha_2 \kappa(\mathbf{y}) G_{n_{\mathbf{y}}n_{\mathbf{y}}} + \alpha_3 \kappa'(\mathbf{y}) G_{\tau_{\mathbf{y}}}$$
(101)

$$K_2 = G_{n_{\mathbf{y}}} \tag{102}$$

where $\kappa'(\mathbf{y}) := \frac{\mathrm{d}}{\mathrm{d}s} \kappa(\mathbf{y}(s))$ is the arclength derivative of curvature and the coefficients α_1, α_2 , and α_3 are given by:

$$\alpha_1 = 2 - \nu \tag{103}$$

$$\alpha_2 = \frac{(-1+\nu)(7+\nu)}{3-\nu} \tag{104}$$

$$\alpha_3 = \frac{(1-\nu)(3+\nu)}{1+\nu} \tag{105}$$

The corresponding identity matrix becomes:

$$\mathbf{D}_{\text{ext}} = \begin{pmatrix} -\frac{1}{2} & 0\\ c_0 \kappa^2(\mathbf{x}) & -\frac{1}{2} \end{pmatrix}, \ \mathbf{x} \in \partial\Omega$$
 (106)

where $c_0 = \frac{(\nu - 1)(\nu + 3)(2\nu - 1)}{2(3 - \nu)}$. For the interior problem, the same choice of kernels results in the following identity part in the integral equation:

$$\mathbf{D}_{\text{int}} = \begin{pmatrix} \frac{1}{2} & 0\\ -c_0 \kappa^2(\mathbf{x}) & \frac{1}{2} \end{pmatrix}, \ \mathbf{x} \in \partial\Omega$$
 (107)

The corresponding kernel functions in the integral equation are:

$$K_{11} = G_{n_{\mathbf{v}}n_{\mathbf{v}}n_{\mathbf{v}}} + \alpha_1 G_{n_{\mathbf{v}}\tau_{\mathbf{v}}\tau_{\mathbf{v}}} + \alpha_2 \kappa(\mathbf{y}) G_{n_{\mathbf{v}}n_{\mathbf{v}}} + \alpha_3 \kappa'(\mathbf{y}) G_{\tau_{\mathbf{v}}}$$

$$\tag{108}$$

$$K_{12} = G_{n_{\mathbf{v}}}$$
 (109)

$$K_{21} = G_{n_{\mathbf{x}}n_{\mathbf{y}}n_{\mathbf{y}}n_{\mathbf{y}}} + \nu G_{\tau_{\mathbf{x}}\tau_{\mathbf{x}}n_{\mathbf{y}}n_{\mathbf{y}}n_{\mathbf{y}}} + \alpha_{1}G_{n_{\mathbf{x}}n_{\mathbf{x}}n_{\mathbf{y}}\tau_{\mathbf{y}}\tau_{\mathbf{y}}} + \nu \alpha_{1}G_{\tau_{\mathbf{x}}\tau_{\mathbf{x}}n_{\mathbf{y}}\tau_{\mathbf{y}}\tau_{\mathbf{y}}} +$$

$$\alpha_2 \kappa(\mathbf{y}) G_{n_{\mathbf{x}} n_{\mathbf{x}} n_{\mathbf{y}} n_{\mathbf{y}}} + \nu \alpha_2 \kappa(\mathbf{y}) G_{\tau_{\mathbf{x}} \tau_{\mathbf{x}} n_{\mathbf{y}} n_{\mathbf{y}}} + \alpha_3 \kappa'(\mathbf{y}) G_{n_{\mathbf{x}} n_{\mathbf{x}} \tau_{\mathbf{y}}} + \nu \alpha_3 \kappa'(\mathbf{y}) G_{\tau_{\mathbf{x}} \tau_{\mathbf{x}} \tau_{\mathbf{y}}}$$
(110)

$$K_{22} = G_{n_{\mathbf{x}}n_{\mathbf{x}}n_{\mathbf{y}}} + \nu G_{\tau_{\mathbf{x}}\tau_{\mathbf{x}}n_{\mathbf{y}}} \tag{111}$$

Theorem 3. For $\nu \notin \{-1,3\}$, the kernels K_{11}, K_{12}, K_{21} , and K_{22} are continuous.

Proof. As before, let $G^B(\mathbf{x}, \mathbf{y}) = \frac{1}{16\pi} |\mathbf{x} - \mathbf{y}|^2 \ln(|\mathbf{x} - \mathbf{y}|^2)$ for $\mathbf{x}, \mathbf{y} \in \partial \Omega$. Since we are taking at most five derivatives, it's sufficient for us to show the continuity of the equivalent kernels of the biharmonic Green's function $K_{11}^B, K_{12}^B, K_{21}^B, K_{22}^B$ as $|\mathbf{x} - \mathbf{y}| \to 0$. Having already appeared in Sections 3 and 4, the kernels in K_{11}^B, K_{12}^B , and K_{22}^B are defined to be continuous on a smooth boundary. It remains to show that K_{21}^B is continuous. The curvature of the boundary at the source point can be expanded as:

$$\kappa(\mathbf{y}) = \kappa(0) + s\kappa'(0) + \frac{1}{2}s^2\kappa''(0) + \mathcal{O}(s^3)$$
(112)

While the arclength derivative of curvature can also be expanded:

$$\kappa'(\mathbf{y}) = \kappa'(0) + s\kappa''(0) + \mathcal{O}(s^2) \tag{113}$$

Using these two expansions, as well as the previous expansions for the normal and tangential derivatives, we obtain the on-surface asymptotics for the terms in K_{21}^B :

$$G_{n_{\mathbf{x}}n_{\mathbf{x}}n_{\mathbf{y}}n_{\mathbf{y}}n_{\mathbf{y}}}^{B}(\mathbf{x}, \mathbf{y}) = -\frac{3\kappa(0)}{4\pi} \frac{1}{s^{2}} - \frac{\kappa'(0)}{\pi} \frac{1}{s} + \frac{3\kappa^{3}(0) - 7\kappa''(0)}{16\pi} + \mathcal{O}(s)$$
(114)

$$G_{\tau_{\mathbf{x}}\tau_{\mathbf{x}}n_{\mathbf{y}}n_{\mathbf{y}}n_{\mathbf{y}}}^{B}(\mathbf{x}, \mathbf{y}) = -\frac{3\kappa(0)}{4\pi} \frac{1}{s^{2}} + \frac{3\kappa^{3}(0) + \kappa''(0)}{16\pi} + \mathcal{O}(s)$$
(115)

$$G_{n_{\mathbf{x}}n_{\mathbf{x}}n_{\mathbf{y}}\tau_{\mathbf{y}}}^{B}(\mathbf{x}, \mathbf{y}) = \frac{5\kappa(0)}{4\pi} \frac{1}{s^{2}} + \frac{\kappa'(0)}{\pi} \frac{1}{s} + \frac{-7\kappa^{3}(0) + 19\kappa''(0)}{48\pi} + \mathcal{O}(s)$$
(116)

$$G_{\tau_{\mathbf{x}}\tau_{\mathbf{x}}n_{\mathbf{y}}\tau_{\mathbf{y}}\tau_{\mathbf{y}}}^{B}(\mathbf{x}, \mathbf{y}) = \frac{\kappa(0)}{4\pi} \frac{1}{s^{2}} - \frac{11\kappa^{3}(0) + \kappa''(0)}{48\pi} + \mathcal{O}(s)$$

$$(117)$$

$$\kappa(\mathbf{y}) G_{n_{\mathbf{x}}n_{\mathbf{x}}n_{\mathbf{y}}n_{\mathbf{y}}}^{B}(\mathbf{x}, \mathbf{y}) = \frac{3\kappa(0)}{4\pi} \frac{1}{s^{2}} + \frac{3\kappa'(0)}{4\pi} \frac{1}{s} + \frac{6\kappa''(0) - 3\kappa^{3}(0)}{16\pi} + \mathcal{O}(s)$$
(118)

$$\kappa(\mathbf{y}) G_{\tau_{\mathbf{x}}\tau_{\mathbf{x}}n_{\mathbf{y}}n_{\mathbf{y}}}^{B}(\mathbf{x}, \mathbf{y}) = -\frac{\kappa(0)}{4\pi} \frac{1}{s^{2}} - \frac{\kappa'(0)}{4\pi} \frac{1}{s} - \frac{6\kappa''(0) - \kappa^{3}(0)}{48\pi} + \mathcal{O}(s)$$
(119)

$$\kappa'(\mathbf{y}) G_{n_{\mathbf{x}}n_{\mathbf{x}}\tau_{\mathbf{y}}}^{B}(0, \mathbf{y}) = \frac{\kappa'(0)}{4\pi} \frac{1}{s} + \frac{\kappa''(0)}{4\pi} + \mathcal{O}(s)$$
(120)

$$\kappa'(\mathbf{y}) G_{\tau_{\mathbf{x}}\tau_{\mathbf{x}}\tau_{\mathbf{y}}}^{B}(0, \mathbf{y}) = \frac{\kappa'(0)}{4\pi} \frac{1}{s} + \frac{\kappa''(0)}{4\pi} + \mathcal{O}(s)$$
(121)

It follows that:

$$\lim_{s \to 0} K_{21}^B(\mathbf{x}, \mathbf{y}) = \frac{(\nu - 1) \left(12\kappa^3 \left(\nu^2 - \nu + 4\right) + \kappa'' \left(-5\nu^2 + 4\nu + 33\right)\right)}{48\pi(\nu - 3)}$$
(122)

Because the boundary $\partial\Omega$ is smooth, the limit is well-defined, and the kernel K_{21}^B is continuous.

Corollary 3. The integral equation associated with (106)-(111) is Fredholm second kind.

Proof. Following the same reasoning as before, the kernels K_{11} , K_{12} , K_{21} , and K_{22} are continuous on surface and therefore the integral operators associated with these kernels are compact. Moreover, **D** is bounded and invertible on a smooth curve.

6. Numerical Implementation

In this section we sketch relevant details for the numerical implementation of the proposed scheme for solving the boundary value problems (8). In subsection 6.1, we briefly discuss the discretization approach we use. Following this, in subsection 6.2 we touch on catastrophic cancellations which arise in a naïve attempt to discretize the integral operators, as well as a method for circumventing these difficulties.

6.1. Details of the discretization

In order to solve boundary integral equations of the form (8), we use a standard modified Nyström method. In particular, the boundary curve $\partial\Omega$ is divided into N_p curved panels, each of which is approximated by a polynomial interpolant at scaled, $n_{\rm GL}$ -th order Gauss-Legendre nodes, for a total of $N=N_pn_{\rm GL}$ boundary nodes; see Figure 1 for an illustration of the discretization nodes with $N_p=4$ and $n_{\rm GL}=16$. Unless otherwise stated, the numerical results are for $n_{\rm GL}=16$. We approximate the boundary layer densities ρ_1, ρ_2 by their polynomial interpolants at the same nodes.

The discrete approximation of (8) is then obtained by enforcing that the integral equation holds at the boundary nodes. Since the integral kernels K_{ij} are in general continuous but not smooth, the integrals in (8) require special quadrature rules to obtain a high order accurate

discretization. Here, we apply special generalized Gaussian quadrature rules [57] (GGQ) which are pre-computed for the class of integral kernels we encounter, specifically integral kernels of the form $\psi(t) + \phi(t) \log |t - t_0|$, where ψ and ϕ are smooth functions and t_0 is a given point.

To visualize the solutions we must also evaluate the integrals in the layer potential representation, (5). For target points, **x**, near the boundary, the integral is nearly-singular. In this case, we approximate the corresponding integrals with high accuracy using adaptive Gaussian integration. For the numerical results presented below, we use the **chunkIE** package in MATLAB [58], which provides utilities for discretizing the curve by panels, applying generalized Gaussian quadrature rules to obtain the discretization of (8), and computing the integrals in the layer potential representation by adaptive quadrature.

6.2. Catastrophic cancellation

While the integral kernels derived in this work are at most weakly singular when restricted to the boundary, a naïve implementation of the integral kernel formulae can lead to catastrophic cancellation. Recall that the Green's function is defined as a scaled difference of the Helmholtz and modified Helmholtz Green's functions, i.e.

$$G(\mathbf{x}, \mathbf{y}) = \frac{1}{2k^2} \left(\frac{i}{4} H_0^{(1)}(k|\mathbf{x} - \mathbf{y}|) - \frac{1}{2\pi} K_0(k|\mathbf{x} - \mathbf{y}|) \right).$$

However, G and its derivatives should not be evaluated by evaluating the $H_0^{(1)}$ and K_0 terms separately and taking the difference for small values of $|k||\mathbf{x}-\mathbf{y}|$. These terms have the same leading order asymptotics for small $|k||\mathbf{x}-\mathbf{y}|$, so G and its derivatives should be evaluated using the appropriate Taylor series [48, §10.8] and explicitly performing the cancellation between these terms, as in (25). In fact, it is convenient to use these power series to write a subroutine which can also evaluate $G(\mathbf{x}, \mathbf{y}) - G^B(\mathbf{x}, \mathbf{y})$ stably for small $|k||\mathbf{x} - \mathbf{y}|$, as we will see below.

Other forms of numerical cancellation can occur in implementing the integral kernels, which are given as linear combinations of the derivatives of G; indeed, such cancellations are necessary to avoid singularities in the integral kernels. Conveniently, up to 5th order derivatives of the quantity $G(\mathbf{x}, \mathbf{y}) - G^B(\mathbf{x}, \mathbf{y})$ are bounded and continuous. Most numerical cancellations can then be mitigated by carefully considering the same linear combinations of G^B .

For example, consider the kernel K_{21} from the clamped plate boundary integral equation:

$$K_{21} = G_{n_{\mathbf{x}}n_{\mathbf{y}}n_{\mathbf{y}}n_{\mathbf{y}}} + 3G_{n_{\mathbf{x}}n_{\mathbf{y}}\tau_{\mathbf{y}}\tau_{\mathbf{y}}}.$$

This kernel is shown to be continuous above but the individual terms are proportional to $1/|\mathbf{x} - \mathbf{y}|^2$. Fortunately, in the biharmonic part K_{21}^B , the cancellations can be carried out explicitly. We have

$$G_{n_{\mathbf{x}}n_{\mathbf{y}}n_{\mathbf{y}}n_{\mathbf{y}}}^{B} + 3G_{n_{\mathbf{x}}n_{\mathbf{y}}\tau_{\mathbf{y}}\tau_{\mathbf{y}}}^{B} = \frac{4}{\pi} \frac{[\mathbf{r} \cdot n(\mathbf{y})]^{3}[\mathbf{r} \cdot n(\mathbf{x})]}{r^{6}} - \frac{3}{\pi} \frac{[\mathbf{r} \cdot n(\mathbf{y})]^{2}[n(y) \cdot n(x)]}{r^{4}},$$

where $\mathbf{r} = \mathbf{x} - \mathbf{y}$ and $r = |\mathbf{r}|$. There is a milder form of numerical cancellation in evaluating $\mathbf{r} \cdot n(\mathbf{y}) = \mathcal{O}(r^2)$, but this did not appear to have a significant effect in the numerical results. A reasonably stable scheme for evaluating K_{21} when $|k||\mathbf{x} - \mathbf{y}|$ is small is then obtained by using the power series to evaluate $(G - G^B)_{n_{\mathbf{x}}n_{\mathbf{y}}n_{\mathbf{y}}n_{\mathbf{y}}} + 3(G - G^B)_{n_{\mathbf{x}}n_{\mathbf{y}}\tau_{\mathbf{y}}\tau_{\mathbf{y}}}$, using a straightforward implementation to evaluate $G^B_{n_{\mathbf{x}}n_{\mathbf{y}}n_{\mathbf{y}}n_{\mathbf{y}}} + 3G^B_{n_{\mathbf{x}}n_{\mathbf{y}}\tau_{\mathbf{y}}\tau_{\mathbf{y}}}$ via the formula above, and then adding the results.

In some cases it is more difficult to carry out the cancellations in the biharmonic part. Consider the kernel K_{21} for the supported plate boundary integral equation:

$$K_{21} = G_{n_{\mathbf{x}}n_{\mathbf{y}}n_{\mathbf{y}}n_{\mathbf{y}}} + \nu G_{\tau_{\mathbf{x}}\tau_{\mathbf{x}}n_{\mathbf{y}}n_{\mathbf{y}}} + \alpha_{1}G_{n_{\mathbf{x}}n_{\mathbf{x}}n_{\mathbf{y}}\tau_{\mathbf{y}}} + \nu \alpha_{1}G_{\tau_{\mathbf{x}}\tau_{\mathbf{x}}n_{\mathbf{y}}\tau_{\mathbf{y}}\tau_{\mathbf{y}}} + \alpha_{2}\kappa(\mathbf{y})G_{n_{\mathbf{x}}n_{\mathbf{x}}n_{\mathbf{y}}n_{\mathbf{y}}} + \nu \alpha_{2}\kappa(\mathbf{y})G_{\tau_{\mathbf{x}}\tau_{\mathbf{x}}n_{\mathbf{y}}n_{\mathbf{y}}} + \alpha_{3}\kappa'(\mathbf{y})G_{n_{\mathbf{x}}n_{\mathbf{x}}\tau_{\mathbf{y}}} + \nu \alpha_{3}\kappa'(\mathbf{y})G_{\tau_{\mathbf{x}}\tau_{\mathbf{x}}\tau_{\mathbf{y}}}.$$

A proper treatment of the numerical cancellations in this kernel for small $|\mathbf{x} - \mathbf{y}|$ would require constructing higher order Taylor series of the coordinates of the curve. In lieu of this, we have instead leveraged the smoothness of the biharmonic part of K_{21} to (partially) mitigate such cancellations.

The idea is to split the kernel into $K_{21} = (K_{21} - K_{21}^B) + K_{21}^B$ as before. For the difference, $(K_{21} - K_{21}^B)$, the power series for $G - G^B$ can be used to stably evaluate the kernel. This component of the kernel is continuous, with limited smoothness owing to the logarithmic terms in the power series. We thus treat this part of the term using a GGQ rule for logarithmic singularities.

To handle K_{21}^B , we observe that the use of a GGQ rule is unnecessary because the kernel is smooth (on a smooth curve). We can instead use a standard Gaussian quadrature rule. This provides a significant improvement in stability which can be understood by analyzing the inter-node spacing and integral weights in each scheme. Consider Gauss-Legendre nodes of order $n_{\rm GL}=16$ scaled to [-1,1]. The smallest inter-node spacing occurs for the node nearest -1, at a distance $\approx 4.5 \times 10^{-2}$ and the corresponding (smooth) integration weight is $\approx 6.2 \times 10^{-2}$. In contrast, the GGQ rule we apply for functions with logarithmic singularities uses support nodes which are specific to each "target" Gauss-Legendre node. For the node of order $n_{\rm GL}=16$ that is closest to -1, the closest support node is at a distance of $\approx 2.2 \times 10^{-4}$ with a weight of $\approx 2.4 \times 10^{-3}$. Because we expect to lose precision proportional to the product of the integral weight and the inverse square of the inter-node distance (when using an unstable evaluator for K_{21}^B), we expect that the standard rule will yield higher precision and this is observed in practice.

7. Results

In order to test the error of these methods, we place a point source inside the domain and set the righthand side of the integral equation to be the point source evaluated using the appropriate boundary conditions. Because the field resulting from this point source satisfies the flexural wave equation, the integral equation should reconstruct the Green's function outside the domain. We refer to this test as the analytic solution test, since the analytic expression for the Green's function is known.

To test the convergence of these methods, we solve the BIE on a "droplet" shaped domain (Figure 1), which is parametrized by the equations:

$$x(t) = 2\cos(t) \tag{123}$$

$$y(t) = \sin(t) - 0.4\cos^2(t) \tag{124}$$

with $t \in [0, 2\pi)$. This domain was chosen because it has non-constant curvature and one fewer axis of symmetry than an ellipse. The source was placed inside the domain at the point (x, y) = (0.8, 0.5), which is off-center to avoid any savings that may result from symmetries in the domain. Finally, the error was measured at a collection of twelve points that come from the augmented domain $\frac{3}{2}(x(t), y(t))$, where $t = n\pi/6$ for n = 1, ..., 12. To compute the relative error, the ℓ_{∞} error at the collection of points is calculated and then divided by the sums of the L_1 norms of the densities on the boundary.

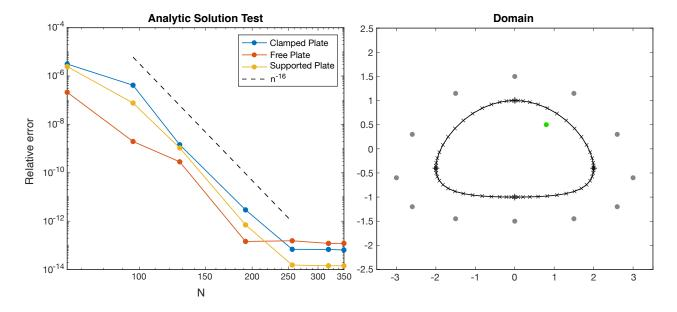


Figure 1: Convergence of the three boundary integral equations ($k=8,\nu=1/3$) as a function of the number of discretization points. The solutions converge at sixteenth order using a combination of smooth and log quadratures. The solutions were solved on a domain shaped like a droplet (right), with the green dot representing the location of the point source and the grey dots representing the locations where the error was measured. The discretization on the right uses four 16-point Gauss-Legendre panels, which was the coarsest discretization that was tested.

To investigate the qualitative differences in different boundary conditions, we plot the far-field patterns that are generated when a wave is scattered by an object, in this case, a tripedal starfish (Figure 2). The parametrization for a generic starfish is given by

$$x(t) = x_0 + (1 + A\cos(nt))\cos(t) \tag{125}$$

$$y(t) = y_0 + (1 + A\cos(nt))\sin(t)$$
(126)

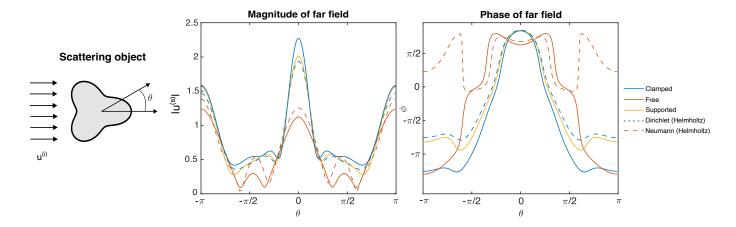


Figure 2: Comparison of boundary conditions on a starfish for wavenumber k=3. Different boundary conditions lead to different far field patterns. The clamped plate creates the darkest shadow and the strongest backscatter. Meanwhile, in the free plate, the shadow and the backscatter are roughly equal in magnitude. The far field pattern generated by the supported plate is notably similar to that generated by the Helmholtz equation with Dirichlet boundary conditions.

where $t \in [0, 2\pi)$, the size of the arms is given by A, the center of the starfish is given by (x_0, y_0) , and the number of appendages is given by n (in this case n = 3). We let the incoming field be $u^{(i)}(\mathbf{x}) := e^{i\mathbf{k}\cdot\mathbf{x}}$ where $\mathbf{k} = (3, 0)$ and set the boundary conditions for the scattered field, $u^{(s)}$ to be the negative of the boundary data corresponding to the plane wave, so that the boundary data of the total field, $u = u^{(i)} + u^{(s)}$, is equal to zero. Because the Yukawa part of the Green's function (4) decays exponentially away from the boundary, the solutions far away from the boundary will naturally look like solutions to the Helmholtz equation. The limiting behavior of the two-dimensional Helmholtz Green's function is $H_0^{(1)}(k|\mathbf{x}|) \sim \sqrt{\frac{2}{\pi k|\mathbf{x}|}} e^{i(k|\mathbf{x}|-\frac{1}{4}\pi)}$ [48], therefore the far-field pattern of the Helmholtz scattering problem can be written as $u^{(s)} \sim f(\theta) \frac{1}{|\mathbf{x}|} e^{ik|\mathbf{x}|}$. Taking $|\mathbf{x}|$ sufficiently large to guarantee we are in the Helmholtz regime and multiplying the scattered field by $|\mathbf{x}|e^{-ik|\mathbf{x}|}$, we can easily recover the far-field pattern $f(\theta)$. To understand how the solutions to flexural wave BVPs differ from Helmholtz, we also plot the far field patterns for the Helmholtz scattering problem with Dirichlet and Neumann boundary conditions. Lastly, the phase of the outgoing solutions is calculated using the formula $\phi = \arctan(\Im(u^{(s)})/\Re(u^{(s)}))$.

The selection of boundary conditions leads to qualitatively different patterns in the far-field (Figures 2 and 3). The clamped plate has a disruptive effect on the incoming wave, leading to the darkest shadow and the strongest backscatter. This effect is even stronger than the analogous Dirichlet problem for the Helmholtz equation. Meanwhile, the free plate had the lightest shadow and weakest backscatter, suggesting that the wave is able to "pass" through the object with less disturbance. Again, this passivity is stronger in the flexural wave case than in the analogous Neumann problem for the Helmholtz equation. The far field of the supported plate is surprisingly similar to that of the Dirichlet problem for the Helmholtz equation.

The phase of the far field varies to an even greater extent than the magnitude. In some parts of the far-field ($\theta = \pm \pi/2$), the clamped and free plate are roughly half a period out of phase, while in other parts of the far-field ($\theta = \pi$), the clamped and far fields are in phase. This is a large contrast from the Helmholtz case, where the Dirichlet and Neumann problems are once again half a period out of phase at the angle $\theta = \pi$.

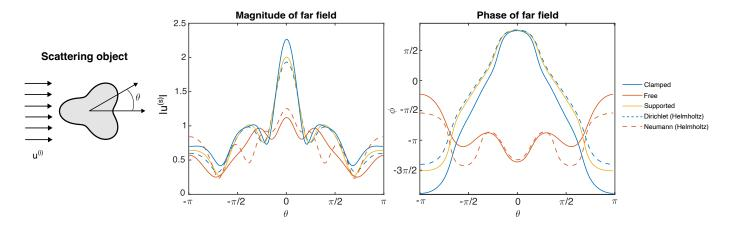


Figure 3: Far field patterns generated by the same wavenumber and starfish rotated by $\pi/3$. Again, the wavenumber is k=3. In this case, the backscatter is not quite as strong due to the change in the orientation in the starfish. Instead, there is one main peak corresponding to the shadow and two smaller peaks corresponding to waves which are deflected off of the arms of the starfish. Again, the far field pattern of the supported plate is similar to the far field pattern of the Helmholtz equation with Dirichlet boundary conditions.

A convenient feature of the boundary integral equations described in this paper is that, after suitable discretization, they are amenable to standard techniques from fast algorithms such as *inter alia* fast multipole methods [59, 60, 61, 62, 63, 64, 65, 66], and fast direct solvers [67, 68, 69, 70, 71, 67, 72, 73, 74, 75, 76, 77, 78, 79, 80, 81, 82, 83, 84, 85, 86, 87, 88, 89]. As a demonstration of this, we conclude our numerical illustrations with an example of the BIE applied to a large scale problem. In particular, we consider a plane wave scattering off of 101 inclusions with free plate boundary conditions. The resulting discretized system has 76,480 unknowns. To accelerate the computation and reduce the overall memory cost we use a simplified (and slightly modified) version of skeletonization with proxy surfaces, see for example [77]. The results are shown in Figure 4. We remark that a 'branching' structure is visible in the magnitude of the field. For simpler models this structure has been previously observed both experimentally and numerically in the context of flexural waves [90, 91, 92, 93]. Our formulation allows for further exploration of this phenomenon.

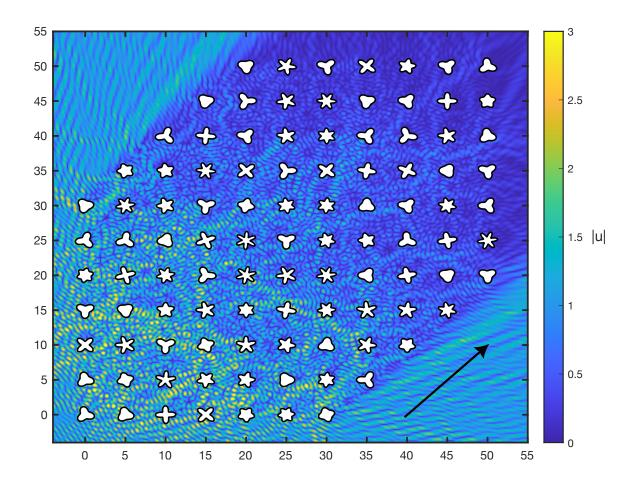


Figure 4: Flexural wave scattering by a collection of 101 starfish-shaped cavities in a thin elastic plate. Free plate BCs are prescribed on the boundary of each starfish, allowing the wave to pass quite far into the array before being attenuated. The wavenumber of the incident wave is k = 6 and the angle of the incident wave $(\theta = \pi/4)$ is depicted by the black arrow.

8. Discussion

In this paper, we have presented integral equation methods for solving flexural wave problems for three common sets of boundary conditions, either by extending existing methods as in the case of the clamped and supported plates, or by developing new methods in the case of the free plate. For the latter, we have used an integral representation that incorporates the composition of a standard layer potential with the Hilbert transform in order to obtain a second kind integral equation. Since the Hilbert transform offers another set of options for kernels in the integral representation, we believe this method may be useful more generally for the development of new integral representations for BVPs. Though not the focus of this study, interior problems can also be accurately solved using these methods. Given a compact geometry, one can find its interior resonant modes by computing the roots of the Fredholm determinant [94, 95]. Further, the representations should be applicable to the static (k = 0) case, a classical model in elasticity.

Our hope is that these methods will be useful to researchers interested in flexural waves in both the applied engineering and glaciological communities. The methods are high-order accurate and can be readily extended to larger systems using existing fast algorithms. The evolution of sea ice and ice shelves is a multiscale phenomenon, and there is a growing desire to model coupled problems at multiple scales [96]. In order to understand how smaller processes involving ice-shelf flexure may have an effect on the the large-scale climate, it is necessary to be able to solve large problems quickly. Fast algorithms based on second-kind integral equation representations are well-equipped to handle these large scattering problems, and we expect these methods to be effective in modeling wave propagation in sea ice and ice shelves. We anticipate that this paper will be the first in a series that leverages integral equations to solve wave scattering problems related to the modeling of sea ice.

The boundary integral equations derived above were shown to be second kind for sufficiently smooth geometries, requiring up to four absolutely continuous derivatives in the boundary parameterization for the Taylor series estimates. There are a number of further questions to explore, including the behavior of the representations on geometries of lower regularity; the solvability of the boundary integral equations and whether or not they are subject to spurious resonances or spurious near-resonances [94]; and the uniqueness properties of solutions to the exterior free plate problem. The authors plan to explore the development of representations for these problems with weaker dependence on the smoothness of the curve. Such representations may be necessary for the treatment of domains with geometric singularities, like corners and cracks. The solvability of the integral equations will be treated in future work, including the characterization of any nullspaces and resonances of the equations for both the $k \neq 0$ and k = 0 cases. The application of these methods to transmitting flexural waves is also being vigorously pursued.

9. Code availability

The integral equations were implemented and solved in ChunkIE, a MATLAB integral equations toolbox (https://github.com/fastalgorithms/chunkie). The examples from this paper may be found at https://github.com/askhamwhat/flex-paper-examples.

10. Acknowledgements

We would like to thank Douglas MacAyeal, Shidong Jiang, Tristan Goodwill, and Mary Silber for many useful discussions. P.N. would like to acknowledge the support of the National Science Foundation (NSF) under Grant No. 2332479. J.G. Hoskins would like to thank the American Institute of Mathematics and, in particular, John Fry for hosting him on Bock Cay during the SQuaREs program, where parts of this work were completed.

Appendix A. Heuristic strategy for deriving the integral kernels

Here we review the strategy mentioned in [1] for deriving suitable integral kernels K_i and describe its extension to the free and supported plate problems. In order to derive the kernels, it is useful to look at the Green's function on a domain with infinitely many degrees of symmetry. Consider the upper half-plane $\Omega := \{(x_1, x_2) | x_2 \ge 0\}$. In this geometry, the convolutions that define layer potentials can be understood in terms of the Fourier transforms of the integral kernels in the x_1 direction; for an application, see [97]. The Green's function has the Sommerfeld integral identity [98]:

$$G(\mathbf{x}, \mathbf{y}) = \int_{-\infty}^{\infty} \hat{G}(\xi, x_2) \exp\left(i\xi(x_1 - y_1)\right) d\xi \tag{A.1}$$

where

$$\hat{G}(\xi, x_2) = \frac{1}{8\pi k^2} \left(\frac{\exp\left(-x_2\sqrt{\xi^2 - k^2}\right)}{\sqrt{\xi^2 - k^2}} - \frac{\exp\left(-x_2\sqrt{\xi^2 + k^2}\right)}{\sqrt{\xi^2 + k^2}} \right)$$
(A.2)

given $\mathbf{x} = (x_1, x_2)$ and $\mathbf{y} = (y_1, 0)$. Because the expression for \hat{G} is separated in the x_1 and x_2 directions, it is simple to compute a similar Fourier transform of normal and tangential derivatives of the Green's function.

For any candidate kernel, K_i , given as some linear combination of derivatives of the Green's function, it is then possible to evaluate the $x_2 \to 0^+$ limit of the boundary conditions applied to that kernel in terms of its Fourier transform. Generally, the asymptotic expansion of this limit will include terms of the form ξ^m or $\xi^m \operatorname{sign}(\xi)$ for $m \in \mathbb{Z}$ as $\xi \to \pm \infty$ which can be used to characterize the corresponding boundary integral operator: positive values of m correspond to hyper-singular boundary integral kernels in the \mathbf{K} matrix or differential operators in the \mathbf{D} matrix and a non-zero constant term in the expansion corresponds to a constant jump while a signed constant corresponds to a Hilbert transform. The goal in integral kernel design is that this limiting system should be second kind. Ideally, $D_{ii} + K_{ii}$ should have a constant term and no higher order terms in the asymptotic expansion while $D_{ij} + K_{ij}$ for $i \neq j$ should have only o(1) terms.

For example, the $\xi \to \pm \infty$ asymptotic expansions of some derivatives of G are below

$$\lim_{x_2 \to 0^+} \widehat{G_{n_{\mathbf{y}} n_{\mathbf{y}} n_{\mathbf{y}}}} = \frac{1}{2} + o(1)$$
(A.3)

$$\lim_{x_2 \to 0^+} \widehat{G_{n_{\mathbf{y}}\tau_{\mathbf{y}}\tau_{\mathbf{y}}}} = 0 + o(1) \tag{A.4}$$

$$\lim_{x_2 \to 0^+} \widehat{G_{n_{\mathbf{x}}n_{\mathbf{y}}n_{\mathbf{y}}n_{\mathbf{y}}}} = \frac{3}{4}|\xi| + o(1)$$
(A.5)

$$\lim_{x_2 \to 0^+} \widehat{G_{n_{\mathbf{x}} n_{\mathbf{y}} \tau_{\mathbf{y}} \tau_{\mathbf{y}}}} = -\frac{1}{4} |\xi| + o(1) . \tag{A.6}$$

From these, we see that the K_1 kernel for the clamped plate problem, $K_1 = G_{n_{\mathbf{y}}n_{\mathbf{y}}n_{\mathbf{y}}} + 3G_{n_{\mathbf{y}}\tau_{\mathbf{y}}\tau_{\mathbf{y}}}$, should have

$$\widehat{D_{11} + K_{11}} = \frac{1}{2} + o(1) \tag{A.7}$$

$$\widehat{D_{21} + K_{21}} = o(1) , \qquad (A.8)$$

as desired.

Here we make a few observations. The first is that this analysis predicts, correctly, that $D_{11} + \mathcal{K}_{11}$ should be second kind, with the constant in the Fourier transform corresponding to the interior jump for this geometry. The second is that the curvature-dependent term in $D_{21} + \mathcal{K}_{21}$ is not predicted because the boundary is flat. Finally, we note that it is a general fact that the asymptotic expansions contain terms of the form ξ^m if the number of normal derivatives is odd and of the form $\xi^m \operatorname{sign}(\xi)$ if the number is even. That is why the linear combination of a term with three normal derivatives and a term with one normal derivative is able to achieve cancellations in the singular parts.

The effect of curvature can be better understood by considering the analogous problem on the disk, where the Fourier series of the Green's function can be written using Graf's addition formula:

$$G(\mathbf{x}, \mathbf{y}) = \frac{1}{2k^2} \sum_{n=-\infty}^{\infty} \left[\frac{i}{4} H_n^{(1)}(kr_{\mathbf{x}}) J_n(kr_{\mathbf{y}}) - \frac{1}{2\pi} K_n(kr_{\mathbf{x}}) I_n(kr_{\mathbf{y}}) \right] \exp(in\alpha)$$
(A.9)

subject to $r_{\mathbf{x}} > r_{\mathbf{y}}$, where $r_{\mathbf{x}}$ is the target radius, $r_{\mathbf{y}}$ is the source radius, and α is the angle between the source and the target. As above, the separated representation allows for relatively straightforward calculations of normal and tangential derivatives. The asymptotic expansions (as $n \to \pm \infty$) of the Fourier coefficients can then be computed and a similar analysis applied. If the disk radius, $r_{\mathbf{y}}$, appears in the asymptotics, this corresponds to a curvature dependence. This can help guide the derivation of the jump conditions on general curves.

For the free plate problem, we use a slightly different representation of the form $\mathcal{K}_1 = \mathcal{K}_1^a + \mathcal{K}_1^b \mathcal{H}$. Because the Fourier symbol of the Hilbert transform is $-i \operatorname{sign}(\xi)$, such a representation allows us to cancel the singular parts of K_1^a and K_1^b , even though K_1^a has one normal derivative and K_1^b has none. As observed in Section 4, this effect can be understood for general curves by applying the Poincaré-Bertrand formula and adding and subtracting the Hilbert transform from appropriate parts of the kernel. This Hilbert transform-based strategy then gives new degrees of freedom in the design of integral kernels on general curves and surfaces and is likely applicable to integral kernel design for a variety of problems.

Appendix B. Formulae for the derivatives of the biharmonic Green's function

Let us denote the biharmonic Green's function as $G^B = \frac{1}{16\pi} \mathbf{r}^2 \ln(\mathbf{r}^2)$, where $\mathbf{r}^2 = \mathbf{r} \cdot \mathbf{r}$ and $\mathbf{r} = \mathbf{x} - \mathbf{y}$ is the distance between the target and the source. For the sake of completeness, we provide formulae for the derivatives of the biharmonic Green's function, which are used to analyze the leading order behavior of the flexural wave kernels:

Appendix B.1. Clamped plate kernels

First, we provide the following derivatives of G^B used in the integral equation for the clamped plate (Theorem 1).

$$G_{n_{\mathbf{y}}n_{\mathbf{y}}}^{B} = \frac{1}{4\pi} \frac{[\boldsymbol{r} \cdot n(\mathbf{y})]^{2}}{\boldsymbol{r}^{2}} + \frac{1}{8\pi} \ln(\boldsymbol{r}^{2}) + \frac{1}{8\pi}$$
(B.1)

$$G_{\tau_{\mathbf{y}}\tau_{\mathbf{y}}}^{B} = \frac{1}{4\pi} \frac{[\mathbf{r} \cdot \tau(\mathbf{y})]^{2}}{\mathbf{r}^{2}} + \frac{1}{8\pi} \ln(\mathbf{r}^{2}) + \frac{1}{8\pi}$$
(B.2)

$$G_{n_{\mathbf{x}}n_{\mathbf{y}}n_{\mathbf{y}}}^{B} = \frac{1}{2\pi} \frac{[\mathbf{r} \cdot n(\mathbf{y})][n(\mathbf{y}) \cdot n(\mathbf{x})]}{\mathbf{r}^{2}} - \frac{1}{2\pi} \frac{[\mathbf{r} \cdot n(\mathbf{x})][\mathbf{r} \cdot n(\mathbf{y})]^{2}}{\mathbf{r}^{4}} + \frac{1}{4\pi} \frac{\mathbf{r} \cdot n(\mathbf{x})}{\mathbf{r}^{2}}$$
(B.3)

$$G_{n_{\mathbf{x}}\tau_{\mathbf{y}}\tau_{\mathbf{y}}}^{B} = \frac{1}{2\pi} \frac{[\mathbf{r} \cdot \tau(\mathbf{y})][\tau(\mathbf{y}) \cdot n(\mathbf{x})]}{\mathbf{r}^{2}} - \frac{1}{2\pi} \frac{[\mathbf{r} \cdot n(\mathbf{x})][\mathbf{r} \cdot \tau(\mathbf{y})]^{2}}{\mathbf{r}^{4}} + \frac{1}{4\pi} \frac{\mathbf{r} \cdot n(\mathbf{x})}{\mathbf{r}^{2}}$$
(B.4)

$$G_{n_{\mathbf{y}}n_{\mathbf{y}}n_{\mathbf{y}}}^{B} = -\frac{3}{4\pi} \frac{[\mathbf{r} \cdot n(\mathbf{y})]}{\mathbf{r}^{2}} + \frac{1}{2\pi} \frac{[\mathbf{r} \cdot n(\mathbf{y})]^{3}}{\mathbf{r}^{4}}$$
(B.5)

$$G_{n_{\mathbf{y}}\tau_{\mathbf{y}}\tau_{\mathbf{y}}}^{B} = \frac{1}{2\pi} \frac{[\mathbf{r} \cdot n(\mathbf{y})][\mathbf{r} \cdot \tau(\mathbf{y})]^{2}}{\mathbf{r}^{4}} - \frac{1}{4\pi} \frac{\mathbf{r} \cdot n(\mathbf{y})}{\mathbf{r}^{2}}$$
(B.6)

$$G_{n_{\mathbf{x}}n_{\mathbf{y}}n_{\mathbf{y}}n_{\mathbf{y}}}^{B} = -\frac{3}{4\pi} \frac{n(\mathbf{x}) \cdot n(\mathbf{y})}{\mathbf{r}^{2}} + \frac{3}{2\pi} \frac{[\mathbf{r} \cdot n(\mathbf{y})][\mathbf{r} \cdot n(\mathbf{x})]}{\mathbf{r}^{4}} + \frac{3}{2\pi} \frac{[\mathbf{r} \cdot n(\mathbf{y})]^{2}[n(\mathbf{x}) \cdot n(\mathbf{y})]}{\mathbf{r}^{4}} - \frac{2}{\pi} \frac{[\mathbf{r} \cdot n(\mathbf{y})]^{3}[\mathbf{r} \cdot n(\mathbf{x})]}{\mathbf{r}^{6}}$$
(B.7)

$$G_{n_{\mathbf{x}}n_{\mathbf{y}}\tau_{\mathbf{y}}\mathbf{y}}^{B} = \frac{1}{2\pi} \frac{[n(\mathbf{x}) \cdot n(\mathbf{y})][\mathbf{r} \cdot \tau(\mathbf{y})]^{2}}{\mathbf{r}^{4}} + \frac{1}{\pi} \frac{[\mathbf{r} \cdot n(\mathbf{y})][\mathbf{r} \cdot \tau(\mathbf{y})][n(\mathbf{x}) \cdot \tau(\mathbf{y})]}{\mathbf{r}^{4}} - \frac{2}{\pi} \frac{[\mathbf{r} \cdot n(\mathbf{y})][\mathbf{r} \cdot \tau(\mathbf{y})]^{2}[\mathbf{r} \cdot n(\mathbf{x})]}{\mathbf{r}^{6}} - \frac{1}{4\pi} \frac{n(\mathbf{x}) \cdot n(\mathbf{y})}{\mathbf{r}^{2}} + \frac{1}{2\pi} \frac{[\mathbf{r} \cdot n(\mathbf{y})][\mathbf{r} \cdot n(\mathbf{x})]}{\mathbf{r}^{4}}$$
(B.8)

Appendix B.2. Free plate kernels

First, we provide the following derivatives of G^B used in the integral equation for the clamped plate (Theorem 2).

$$G_{n_{\mathbf{x}}n_{\mathbf{x}}}^{B} = \frac{1}{4\pi} \frac{[\mathbf{r} \cdot n(\mathbf{x})]^{2}}{\mathbf{r}^{2}} + \frac{1}{8\pi} \ln(\mathbf{r}^{2}) + \frac{1}{8\pi}$$
(B.9)

$$G_{\tau_{\mathbf{x}}\tau_{\mathbf{x}}}^{B} = \frac{1}{4\pi} \frac{[\mathbf{r} \cdot \tau(\mathbf{x})]^{2}}{\mathbf{r}^{2}} + \frac{1}{8\pi} \ln(\mathbf{r}^{2}) + \frac{1}{8\pi}$$
(B.10)

$$G_{n_{\mathbf{x}}n_{\mathbf{x}}n_{\mathbf{y}}}^{B} = -\frac{1}{2\pi} \frac{[\mathbf{r} \cdot n(\mathbf{x})][n(\mathbf{x}) \cdot n(\mathbf{y})]}{\mathbf{r}^{2}} + \frac{1}{2\pi} \frac{[\mathbf{r} \cdot n(\mathbf{y})][\mathbf{r} \cdot n(\mathbf{x})]^{2}}{\mathbf{r}^{4}} - \frac{1}{4\pi} \frac{\mathbf{r} \cdot n(\mathbf{y})}{\mathbf{r}^{2}}$$
(B.11)

$$G_{\tau_{\mathbf{x}}\tau_{\mathbf{x}}n_{\mathbf{y}}}^{B} = -\frac{1}{2\pi} \frac{[\mathbf{r} \cdot \tau(\mathbf{x})][\tau(\mathbf{x}) \cdot n(\mathbf{y})]}{\mathbf{r}^{2}} + \frac{1}{2\pi} \frac{[\mathbf{r} \cdot n(\mathbf{y})][\mathbf{r} \cdot \tau(\mathbf{x})]^{2}}{\mathbf{r}^{4}} - \frac{1}{4\pi} \frac{\mathbf{r} \cdot n(\mathbf{y})}{\mathbf{r}^{2}}$$
(B.12)

$$G_{n_{\mathbf{x}}n_{\mathbf{x}}\tau_{\mathbf{y}}}^{B} = -\frac{1}{2\pi} \frac{[\mathbf{r} \cdot n(\mathbf{x})][n(\mathbf{x}) \cdot \tau(\mathbf{y})]}{\mathbf{r}^{2}} + \frac{1}{2\pi} \frac{[\mathbf{r} \cdot \tau(\mathbf{y})][\mathbf{r} \cdot n(\mathbf{x})]^{2}}{\mathbf{r}^{4}} - \frac{1}{4\pi} \frac{\mathbf{r} \cdot \tau(\mathbf{y})}{\mathbf{r}^{2}}$$
(B.13)

$$G_{\tau_{\mathbf{x}}\tau_{\mathbf{x}}\tau_{\mathbf{y}}}^{B} = -\frac{1}{2\pi} \frac{[\mathbf{r} \cdot \tau(\mathbf{x})][\tau(\mathbf{x}) \cdot \tau(\mathbf{y})]}{\mathbf{r}^{2}} + \frac{1}{2\pi} \frac{[\mathbf{r} \cdot \tau(\mathbf{y})][\mathbf{r} \cdot \tau(\mathbf{x})]^{2}}{\mathbf{r}^{4}} - \frac{1}{4\pi} \frac{\mathbf{r} \cdot \tau(\mathbf{y})}{\mathbf{r}^{2}}$$
(B.14)

$$G_{n_{\mathbf{x}}n_{\mathbf{x}}n_{\mathbf{x}}}^{B} = \frac{3}{4\pi} \frac{\mathbf{r} \cdot n(\mathbf{x})}{\mathbf{r}^{2}} - \frac{1}{2\pi} \frac{[\mathbf{r} \cdot n(\mathbf{x})]^{3}}{\mathbf{r}^{4}}$$
(B.15)

$$G_{n_{\mathbf{x}}\tau_{\mathbf{x}}\tau_{\mathbf{x}}}^{B} = -\frac{1}{2\pi} \frac{[\mathbf{r} \cdot n(\mathbf{x})][\mathbf{r} \cdot \tau(\mathbf{x})]^{2}}{\mathbf{r}^{4}} + \frac{1}{4\pi} \frac{\mathbf{r} \cdot n(\mathbf{x})}{\mathbf{r}^{2}}$$
(B.16)

$$G_{n_{\mathbf{x}}n_{\mathbf{x}}n_{\mathbf{y}}}^{B} = -\frac{3}{4\pi} \frac{n(\mathbf{x}) \cdot n(\mathbf{y})}{\mathbf{r}^{2}} + \frac{3}{2\pi} \frac{[\mathbf{r} \cdot n(\mathbf{y})][\mathbf{r} \cdot n(\mathbf{x})]}{\mathbf{r}^{4}} + \frac{3}{2\pi} \frac{[\mathbf{r} \cdot n(\mathbf{x})]^{2}[n(\mathbf{x}) \cdot n(\mathbf{y})]}{\mathbf{r}^{4}} - \frac{2}{\pi} \frac{[\mathbf{r} \cdot n(\mathbf{x})]^{3}[\mathbf{r} \cdot n(\mathbf{y})]}{\mathbf{r}^{6}}$$
(B.17)

$$G_{n_{\mathbf{x}}\tau_{\mathbf{x}}n_{\mathbf{y}}}^{B} = \frac{1}{2\pi} \frac{[\mathbf{r} \cdot \tau(\mathbf{x})]^{2}[n(\mathbf{x}) \cdot n(\mathbf{y})]}{\mathbf{r}^{4}} + \frac{1}{\pi} \frac{[\mathbf{r} \cdot \tau(\mathbf{x})][\tau(\mathbf{x}) \cdot n(\mathbf{y})][\mathbf{r} \cdot n(\mathbf{x})]}{\mathbf{r}^{4}} - \frac{2}{\pi} \frac{[\mathbf{r} \cdot n(\mathbf{y})][\mathbf{r} \cdot n(\mathbf{x})][\mathbf{r} \cdot n(\mathbf{x})]^{2}}{\mathbf{r}^{6}} - \frac{1}{4\pi} \frac{n(\mathbf{x}) \cdot n(\mathbf{y})}{\mathbf{r}^{2}} + \frac{1}{2\pi} \frac{[\mathbf{r} \cdot n(\mathbf{y})][\mathbf{r} \cdot n(\mathbf{x})]}{\mathbf{r}^{4}}$$
(B.18)

$$G_{n_{\mathbf{x}}n_{\mathbf{x}}n_{\mathbf{x}}\tau_{\mathbf{y}}}^{B} = -\frac{3}{4\pi} \frac{n(\mathbf{x}) \cdot \tau(\mathbf{y})}{\mathbf{r}^{2}} + \frac{3}{2\pi} \frac{[\mathbf{r} \cdot n(\mathbf{x})][\mathbf{r} \cdot \tau(\mathbf{y})]}{\mathbf{r}^{4}} + \frac{3}{2\pi} \frac{[\mathbf{r} \cdot n(\mathbf{x})]^{2}(n(\mathbf{x}) \cdot \tau(\mathbf{y}))}{\mathbf{r}^{4}} - \frac{2}{\pi} \frac{[\mathbf{r} \cdot \tau(\mathbf{y})][\mathbf{r} \cdot n(\mathbf{x})]^{3}}{\mathbf{r}^{6}}$$
(B.19)

$$G_{n_{\mathbf{x}}\tau_{\mathbf{x}}\tau_{\mathbf{y}}}^{B} = \frac{1}{\pi} \frac{[\mathbf{r} \cdot n(\mathbf{x})][\mathbf{r} \cdot \tau(\mathbf{x})][\tau(\mathbf{x}) \cdot \tau(\mathbf{y})]}{\mathbf{r}^{4}} + \frac{1}{2\pi} \frac{(\tau(\mathbf{y}) \cdot n(\mathbf{x}))[\mathbf{r} \cdot \tau(\mathbf{x})]^{2}}{\mathbf{r}^{4}} - \frac{2}{\pi} \frac{[\mathbf{r} \cdot n(\mathbf{x})][\mathbf{r} \cdot \tau(\mathbf{y})][\mathbf{r} \cdot \tau(\mathbf{y})]^{2}}{\mathbf{r}^{6}} - \frac{1}{4\pi} \frac{\tau(\mathbf{y}) \cdot n(\mathbf{x})}{\mathbf{r}^{2}} + \frac{1}{2\pi} \frac{[\mathbf{r} \cdot n(\mathbf{x})][\mathbf{r} \cdot \tau(\mathbf{y})]}{\mathbf{r}^{4}}$$
(B.20)

Appendix B.3. Supported plate kernels

First, we provide the following derivatives of G^B used in the integral equation for the supported plate (Theorem 3).

$$G_{n_{\mathbf{y}}}^{B} = -\frac{1}{8\pi} [\mathbf{r} \cdot n(\mathbf{y})] \ln(\mathbf{r}^{2}) - \frac{1}{8\pi} [\mathbf{r} \cdot n(\mathbf{y})]$$
(B.21)

$$G_{\tau_{\mathbf{y}}}^{B} = -\frac{1}{8\pi} [\mathbf{r} \cdot \tau(\mathbf{y})] \ln(\mathbf{r}^{2}) - \frac{1}{8\pi} [\mathbf{r} \cdot \tau(\mathbf{y})]$$
(B.22)

$$G_{n_{\mathbf{y}}n_{\mathbf{y}}}^{B} = \frac{1}{4\pi} \frac{[\mathbf{r} \cdot n(\mathbf{y})]^{2}}{\mathbf{r}^{2}} + \frac{1}{8\pi} \ln(\mathbf{r}^{2}) + \frac{1}{8\pi}$$
 (B.23)

$$G_{n_{\mathbf{y}}n_{\mathbf{y}}n_{\mathbf{y}}}^{B} = -\frac{3}{4\pi} \frac{[\mathbf{r} \cdot n(\mathbf{y})]}{\mathbf{r}^{2}} + \frac{1}{2\pi} \frac{[\mathbf{r} \cdot n(\mathbf{y})]^{3}}{\mathbf{r}^{4}}$$
(B.24)

$$G_{n_{\mathbf{y}}\tau_{\mathbf{y}}\tau_{\mathbf{y}}}^{B} = \frac{1}{2\pi} \frac{[\mathbf{r} \cdot n(\mathbf{y})][\mathbf{r} \cdot \tau(\mathbf{y})]^{2}}{\mathbf{r}^{4}} - \frac{1}{4\pi} \frac{\mathbf{r} \cdot n(\mathbf{y})}{\mathbf{r}^{2}}$$
(B.25)

$$G_{n_{\mathbf{x}}n_{\mathbf{x}}n_{\mathbf{y}}}^{B} = -\frac{1}{2\pi} \frac{[\mathbf{r} \cdot n(\mathbf{x})][n(\mathbf{x}) \cdot n(\mathbf{y})]}{\mathbf{r}^{2}} + \frac{1}{2\pi} \frac{[\mathbf{r} \cdot n(\mathbf{y})][\mathbf{r} \cdot n(\mathbf{x})]^{2}}{\mathbf{r}^{4}} - \frac{1}{4\pi} \frac{\mathbf{r} \cdot n(\mathbf{y})}{\mathbf{r}^{2}}$$
(B.26)

$$G_{\tau_{\mathbf{x}}\tau_{\mathbf{x}}n_{\mathbf{y}}}^{B} = -\frac{1}{2\pi} \frac{[\mathbf{r} \cdot \tau(\mathbf{x})][\tau(\mathbf{x}) \cdot n(\mathbf{y})]}{\mathbf{r}^{2}} + \frac{1}{2\pi} \frac{[\mathbf{r} \cdot n(\mathbf{y})][\mathbf{r} \cdot \tau(\mathbf{x})]^{2}}{\mathbf{r}^{4}} - \frac{1}{4\pi} \frac{\mathbf{r} \cdot n(\mathbf{y})}{\mathbf{r}^{2}}$$
(B.27)

$$G_{n_{\mathbf{x}}n_{\mathbf{x}}\tau_{\mathbf{y}}}^{B} = -\frac{1}{2\pi} \frac{[\mathbf{r} \cdot n(\mathbf{x})][n(\mathbf{x}) \cdot \tau(\mathbf{y})]}{\mathbf{r}^{2}} + \frac{1}{2\pi} \frac{[\mathbf{r} \cdot \tau(\mathbf{y})][\mathbf{r} \cdot n(\mathbf{x})]^{2}}{\mathbf{r}^{4}} - \frac{1}{4\pi} \frac{\mathbf{r} \cdot \tau(\mathbf{y})}{\mathbf{r}^{2}}$$
(B.28)

$$G_{\tau_{\mathbf{x}}\tau_{\mathbf{x}}\tau_{\mathbf{y}}}^{B} = -\frac{1}{2\pi} \frac{[\mathbf{r} \cdot \tau(\mathbf{x})][\tau(\mathbf{x}) \cdot \tau(\mathbf{y})]}{\mathbf{r}^{2}} + \frac{1}{2\pi} \frac{[\mathbf{r} \cdot \tau(\mathbf{y})][\mathbf{r} \cdot \tau(\mathbf{x})]^{2}}{\mathbf{r}^{4}} - \frac{1}{4\pi} \frac{\mathbf{r} \cdot \tau(\mathbf{y})}{\mathbf{r}^{2}}$$

$$= 1 [n(\mathbf{x}) \cdot n(\mathbf{y})]^{2} - 2 [\mathbf{r} \cdot n(\mathbf{x})][\mathbf{r} \cdot n(\mathbf{y})][n(\mathbf{x}) \cdot n(\mathbf{y})] + 1 1$$
(B.29)

$$G_{n_{\mathbf{x}}n_{\mathbf{x}}n_{\mathbf{y}}n_{\mathbf{y}}}^{B} = \frac{1}{2\pi} \frac{[n(\mathbf{x}) \cdot n(\mathbf{y})]^{2}}{\mathbf{r}^{2}} - \frac{2}{\pi} \frac{[\mathbf{r} \cdot n(\mathbf{x})][\mathbf{r} \cdot n(\mathbf{y})][n(\mathbf{x}) \cdot n(\mathbf{y})]}{\mathbf{r}^{4}} + \frac{1}{4\pi} \frac{1}{\mathbf{r}^{2}}$$
$$- \frac{1}{2\pi} \frac{[\mathbf{r} \cdot n(\mathbf{y})]^{2}}{\mathbf{r}^{4}} + \frac{2}{\pi} \frac{[\mathbf{r} \cdot n(\mathbf{x})]^{2}[\mathbf{r} \cdot n(\mathbf{y})]^{2}}{\mathbf{r}^{6}} - \frac{1}{2\pi} \frac{[\mathbf{r} \cdot n(\mathbf{x})]^{2}}{\mathbf{r}^{4}}$$
(B.30)

$$G_{\tau_{\mathbf{x}}\tau_{\mathbf{x}}n_{\mathbf{y}}n_{\mathbf{y}}}^{B} = \frac{1}{2\pi} \frac{\left[\tau(\mathbf{x}) \cdot n(\mathbf{y})\right]^{2}}{\mathbf{r}^{2}} - \frac{2}{\pi} \frac{\left[\mathbf{r} \cdot \tau(\mathbf{x})\right]\left[\mathbf{r} \cdot n(\mathbf{y})\right]\left[\tau(\mathbf{x}) \cdot n(\mathbf{y})\right]}{\mathbf{r}^{4}} + \frac{1}{4\pi} \frac{1}{\mathbf{r}^{2}} - \frac{1}{2\pi} \frac{\left[\mathbf{r} \cdot n(\mathbf{y})\right]^{2}}{\mathbf{r}^{4}} + \frac{2}{\pi} \frac{\left[\mathbf{r} \cdot \tau(\mathbf{x})\right]^{2}\left[\mathbf{r} \cdot n(\mathbf{y})\right]^{2}}{\mathbf{r}^{6}} - \frac{1}{2\pi} \frac{\left[\mathbf{r} \cdot \tau(\mathbf{x})\right]^{2}}{\mathbf{r}^{4}}$$
(B.31)

$$G_{n_{\mathbf{x}}n_{\mathbf{x}}n_{\mathbf{y}}n_{\mathbf{y}}n_{\mathbf{y}}}^{B} = \frac{3}{2\pi} \frac{\mathbf{r}^{4}}{\mathbf{r}^{4}} - \frac{6}{\pi} \frac{[\mathbf{r} \cdot n(\mathbf{y})][\mathbf{r} \cdot n(\mathbf{x})]^{2}}{\mathbf{r}^{6}} + \frac{3}{\pi} \frac{[\mathbf{r} \cdot n(\mathbf{y})][n(\mathbf{x}) \cdot n(\mathbf{y})]^{2}}{\mathbf{r}^{4}}$$

$$- \frac{12}{\pi} \frac{[\mathbf{r} \cdot n(\mathbf{y})]^{2}[\mathbf{r} \cdot n(\mathbf{x})][n(\mathbf{x}) \cdot n(\mathbf{y})]}{\mathbf{r}^{6}} - \frac{2}{\pi} \frac{[\mathbf{r} \cdot n(\mathbf{y})]^{3}}{\mathbf{r}^{6}}$$

$$+ \frac{12}{\pi} \frac{[\mathbf{r} \cdot n(\mathbf{y})]^{3}[\mathbf{r} \cdot n(\mathbf{x})]^{2}}{\mathbf{r}^{8}} + \frac{3}{\pi} \frac{[\mathbf{r} \cdot n(\mathbf{x})][n(\mathbf{x}) \cdot n(\mathbf{y})]}{\mathbf{r}^{4}}$$
(B.32)

$$G_{\tau_{\mathbf{x}}\tau_{\mathbf{x}}n_{\mathbf{y}}n_{\mathbf{y}}n_{\mathbf{y}}}^{B} = \frac{3}{2\pi} \frac{\mathbf{r} \cdot n(\mathbf{y})}{\mathbf{r}^{4}} - \frac{6}{\pi} \frac{[\mathbf{r} \cdot n(\mathbf{y})][\mathbf{r} \cdot \tau(\mathbf{x})]^{2}}{\mathbf{r}^{6}} + \frac{3}{\pi} \frac{[\mathbf{r} \cdot n(\mathbf{y})][\tau(\mathbf{x}) \cdot n(\mathbf{y})]^{2}}{\mathbf{r}^{4}}$$

$$- \frac{12}{\pi} \frac{[\mathbf{r} \cdot n(\mathbf{y})]^{2}[\mathbf{r} \cdot \tau(\mathbf{x})][\tau(\mathbf{x}) \cdot n(\mathbf{y})]}{\mathbf{r}^{6}} - \frac{2}{\pi} \frac{[\mathbf{r} \cdot n(\mathbf{y})]^{3}}{\mathbf{r}^{6}}$$

$$+ \frac{12}{\pi} \frac{[\mathbf{r} \cdot n(\mathbf{y})]^{3}[\mathbf{r} \cdot \tau(\mathbf{x})]^{2}}{8} + \frac{3}{\pi} \frac{[\mathbf{r} \cdot \tau(\mathbf{x})][\tau(\mathbf{x}) \cdot n(\mathbf{y})]}{4}$$
(B.33)

$$G_{n_{\mathbf{x}}n_{\mathbf{x}}n_{\mathbf{y}}\tau_{\mathbf{y}}\tau_{\mathbf{y}}}^{B} = \frac{2}{\pi} \frac{[n(\mathbf{x}) \cdot n(\mathbf{y})][n(\mathbf{x}) \cdot \tau(\mathbf{y})][\mathbf{r} \cdot \tau(\mathbf{y})]}{\mathbf{r}^{4}} - \frac{4}{\pi} \frac{[n(\mathbf{x}) \cdot n(\mathbf{y})][\mathbf{r} \cdot \tau(\mathbf{y})]^{2}[\mathbf{r} \cdot n(\mathbf{x})]}{\mathbf{r}^{6}} + \frac{1}{\pi} \frac{[\mathbf{r} \cdot n(\mathbf{y})][n(\mathbf{x}) \cdot \tau(\mathbf{y})]^{2}}{\mathbf{r}^{4}} - \frac{8}{\pi} \frac{[\mathbf{r} \cdot n(\mathbf{y})][\mathbf{r} \cdot \tau(\mathbf{y})][\mathbf{r} \cdot \tau(\mathbf{y})][n(\mathbf{x}) \cdot \tau(\mathbf{y})]}{\mathbf{r}^{6}} - \frac{2}{\pi} \frac{[\mathbf{r} \cdot n(\mathbf{y})][\mathbf{r} \cdot \tau(\mathbf{y})]^{2}}{\mathbf{r}^{6}} + \frac{12}{\pi} \frac{[\mathbf{r} \cdot n(\mathbf{y})][\mathbf{r} \cdot \tau(\mathbf{y})]^{2}[\mathbf{r} \cdot n(\mathbf{x})]^{2}}{\mathbf{r}^{8}} + \frac{1}{\pi} \frac{[n(\mathbf{x}) \cdot n(\mathbf{y})][\mathbf{r} \cdot n(\mathbf{x})]}{\mathbf{r}^{4}} + \frac{1}{2\pi} \frac{\mathbf{r} \cdot n(\mathbf{y})}{\mathbf{r}^{4}} - \frac{2}{\pi} \frac{[\mathbf{r} \cdot n(\mathbf{y})][\mathbf{r} \cdot n(\mathbf{x})]^{2}}{\mathbf{r}^{6}}$$
(B.34)

$$G_{\tau_{\mathbf{x}}\tau_{\mathbf{x}}n_{\mathbf{y}}\tau_{\mathbf{y}}\mathbf{y}}^{B} = \frac{2}{\pi} \frac{[\tau(\mathbf{x}) \cdot n(\mathbf{y})][\tau(\mathbf{x}) \cdot \tau(\mathbf{y})][\mathbf{r} \cdot \tau(\mathbf{y})]}{\mathbf{r}^{4}} - \frac{4}{\pi} \frac{[\tau(\mathbf{x}) \cdot n(\mathbf{y})][\mathbf{r} \cdot \tau(\mathbf{y})]^{2}[\mathbf{r} \cdot \tau(\mathbf{x})]}{\mathbf{r}^{6}} + \frac{1}{\pi} \frac{[\mathbf{r} \cdot n(\mathbf{y})][\tau(\mathbf{x}) \cdot \tau(\mathbf{y})]^{2}}{\mathbf{r}^{4}} - \frac{8}{\pi} \frac{[\mathbf{r} \cdot n(\mathbf{y})][\mathbf{r} \cdot \tau(\mathbf{y})][\mathbf{r} \cdot \tau(\mathbf{y})][\tau(\mathbf{x}) \cdot \tau(\mathbf{y})]}{\mathbf{r}^{6}} - \frac{2}{\pi} \frac{[\mathbf{r} \cdot n(\mathbf{y})][\mathbf{r} \cdot \tau(\mathbf{y})]^{2}}{\mathbf{r}^{6}} + \frac{12}{\pi} \frac{[\mathbf{r} \cdot n(\mathbf{y})][\mathbf{r} \cdot \tau(\mathbf{y})]^{2}[\mathbf{r} \cdot \tau(\mathbf{x})]^{2}}{\mathbf{r}^{8}}$$

$$+\frac{1}{\pi} \frac{[\tau(\mathbf{x}) \cdot n(\mathbf{y})][\mathbf{r} \cdot \tau(\mathbf{x})]}{\mathbf{r}^4} + \frac{1}{2\pi} \frac{\mathbf{r} \cdot n(\mathbf{y})}{\mathbf{r}^4} - \frac{2}{\pi} \frac{[\mathbf{r} \cdot n(\mathbf{y})][\mathbf{r} \cdot \tau(\mathbf{x})]^2}{\mathbf{r}^6}$$
(B.35)

Appendix C. Derivation of jump conditions of the layer potentials

So that this paper is self-contained, we repeat the derivation of jump conditions here. Given the arc-length parametrization $\gamma(t)$, let $\tau(t) := \tau(\gamma(t))$ and $n(t) := n(\gamma(t))$ be the unit tangent and normal vectors at $\gamma(t)$. Suppose that the target point is in the exterior of the domain while the source point is on the boundary:

$$\mathbf{x} := \boldsymbol{\gamma}(t) + hn(t) \tag{C.1}$$

$$\mathbf{y} := \boldsymbol{\gamma}(t+s) \tag{C.2}$$

As before, we expand $\mathbf{r} = (\mathbf{x} - \mathbf{y})$ as:

$$\mathbf{r} = hn(t) - s\tau(t) + \frac{s^2}{2}\kappa n(t) + \frac{s^3}{6}(\kappa' n(t) + \kappa^2 \tau(t)) - \frac{s^4}{24}((-\kappa'' + \kappa^3)n(t) - 3\kappa\kappa'\tau(t)) + \mathcal{O}(s^5)$$
(C.3)

Next, we substitute expressions (59) and (60) into the derivatives of the biharmonic Green's function. We obtain the following off surface asymptotics:

$$G_{n_{\mathbf{x}}n_{\mathbf{x}}n_{\mathbf{x}}}^{B}(\mathbf{x}, \mathbf{y}) = \frac{3}{4\pi} \frac{h}{h^{2} + s^{2}} - \frac{1}{2\pi} \frac{h^{3}}{(h^{2} + s^{2})^{2}} + O(s^{2})$$
(C.4)

Integrating this kernel against some density $\sigma(\mathbf{y}) := \sigma(\gamma(t+s))$ in some region $[-\delta, \delta]$ along the curve and taking the limit as the target approaches the boundary:

$$\lim_{h \to 0} \int_{-\delta}^{+\delta} G_{n_{\mathbf{x}}n_{\mathbf{x}}n_{\mathbf{x}}}(\mathbf{x}, \mathbf{y}(s)) \sigma(\mathbf{y}(s)) \, \mathrm{d}s$$
 (C.5)

$$= \lim_{h \to 0} \left[\sigma(\mathbf{x}) \int_{-\delta}^{+\delta} \left(\frac{3}{4\pi} \frac{h}{h^2 + s^2} - \frac{1}{2\pi} \frac{h^3}{(h^2 + s^2)^2} \right) ds \right]$$
 (C.6)

$$+ \lim_{h \to 0} \int_{-\delta}^{+\delta} (\sigma(\mathbf{y}) - \sigma(\mathbf{x})) \left(\frac{3}{4\pi} \frac{h}{h^2 + s^2} - \frac{1}{2\pi} \frac{h^3}{(h^2 + s^2)^2} \right) ds \right)$$
 (C.7)

We deal with the second integral first. Because $\sigma(\mathbf{x})$ is continuous, (C.7) can be bounded by:

$$\int_{-\delta}^{+\delta} (\sigma(\mathbf{y}) - \sigma(\mathbf{x})) \left(-\frac{3}{4\pi} \frac{h}{h^2 + s^2} + \frac{1}{2\pi} \frac{h^3}{(h^2 + s^2)^2} \right) ds
\leq 2\delta C \int_{-\delta}^{+\delta} \left(-\frac{3}{4\pi} \frac{h}{h^2 + s^2} + \frac{1}{2\pi} \frac{h^3}{(h^2 + s^2)^2} \right) ds$$
(C.8)

which goes to zero as $\delta \to 0$. Next, we integrate (C.6):

$$\lim_{h \to 0} \left(\sigma(\mathbf{x}) \left(\frac{\delta h}{2\pi (\delta^2 + h^2)} + \frac{1}{\pi} \arctan \frac{\delta}{h} \right) \right) ds = \frac{1}{2} \sigma(\mathbf{x})$$
 (C.9)

Finally, we have the jump condition:

$$\lim_{\mathbf{x} \to \partial\Omega} \int_{\partial\Omega} G_{n_{\mathbf{x}}n_{\mathbf{x}}n_{\mathbf{x}}}(\mathbf{x}, \mathbf{y}) \sigma(\mathbf{y}) \, dS(\mathbf{y}) = \frac{1}{2} \sigma(\mathbf{x}) + \int_{\partial\Omega} G_{n_{\mathbf{x}}n_{\mathbf{x}}n_{\mathbf{x}}}(\mathbf{x}, \mathbf{y}) \sigma(\mathbf{y}) \, dS(\mathbf{y})$$
(C.10)

Similar reasoning can be applied to obtain other jump conditions:

$$\lim_{\mathbf{x} \to \partial\Omega} \int_{\partial\Omega} G_{n_{\mathbf{x}}n_{\mathbf{x}}n_{\mathbf{y}}}(\mathbf{x}, \mathbf{y}) \sigma(\mathbf{y}) \, dS(\mathbf{y}) = -\frac{1}{2} \sigma(\mathbf{x}) + \int_{\partial\Omega} G_{n_{\mathbf{x}}n_{\mathbf{x}}n_{\mathbf{y}}}(\mathbf{x}, \mathbf{y}) \sigma(\mathbf{y}) \, dS(\mathbf{y})$$
(C.11)

$$\lim_{\mathbf{x} \to \partial\Omega} \int_{\partial\Omega} G_{n_{\mathbf{x}}n_{\mathbf{y}}n_{\mathbf{y}}}(\mathbf{x}, \mathbf{y}) \sigma(\mathbf{y}) \, dS(\mathbf{y}) = \frac{1}{2} \sigma(\mathbf{x}) + \int_{\partial\Omega} G_{n_{\mathbf{x}}n_{\mathbf{y}}n_{\mathbf{y}}}(\mathbf{x}, \mathbf{y}) \sigma(\mathbf{y}) \, dS(\mathbf{y})$$
(C.12)

$$\lim_{\mathbf{x} \to \partial\Omega} \int_{\partial\Omega} G_{n_{\mathbf{y}}n_{\mathbf{y}}n_{\mathbf{y}}}(\mathbf{x}, \mathbf{y}) \sigma(\mathbf{y}) \, dS(\mathbf{y}) = -\frac{1}{2} \sigma(\mathbf{x}) + \int_{\partial\Omega} G_{n_{\mathbf{y}}n_{\mathbf{y}}n_{\mathbf{y}}}(\mathbf{x}, \mathbf{y}) \sigma(\mathbf{y}) \, dS(\mathbf{y})$$
(C.13)

where the limits above are taken from the exterior. When taken from the interior, the target variable is defined $\mathbf{x} := \boldsymbol{\gamma}(t) - hn(t)$, and as a result conditions (C.10)-(C.13) inherit a negative sign.

For the fifth derivatives, we are required to expand the denominator to higher order. We have that:

$$\mathbf{r}^2 = h^2 + u^2 \tag{C.14}$$

where

$$u^{2} := g(s)^{2} := (1 + h\kappa)s^{2} + \frac{1}{3}h\kappa's^{3} + \frac{1}{12}(h\kappa'' - h\kappa^{3} - \kappa^{2})s^{4} + \mathcal{O}(s^{5})$$
 (C.15)

Inverting this series we have:

$$g^{-1}(u) = \frac{1}{\sqrt{1+hk}}u - \frac{h\kappa'}{6(1+h\kappa)^2}u^2 + \frac{36\kappa^2 + 39h\kappa^3 + 3h^2\kappa^4 + h(5h\kappa'^2 - 3\kappa'') - 3h^2\kappa\kappa''}{72(1+h\kappa)^{7/2}}u^3 + \mathcal{O}(u^4)$$
 (C.16)

Since h is decreasing faster than u, we can further expand each of the coefficients as:

$$g^{-1}(u) = \left(1 - \frac{h\kappa}{2} + \frac{3h^2\kappa^2}{8} - \frac{5h^3\kappa^3}{16} + \frac{35h^4\kappa^4}{128} + \mathcal{O}(h^5)\right)u$$

$$+ \left(-\frac{h\kappa'}{6} + \frac{1}{6}h^2\kappa^2\kappa' - \frac{1}{6}h^3\kappa^4\kappa' + \mathcal{O}(h^4)\right)u^2$$

$$+ \left(\frac{\kappa^2}{2} - \frac{h}{72}(87\kappa^3 + 3\kappa'') + \frac{5}{144}h^2(60\kappa^4 + 2\kappa'^2 + 3\kappa\kappa'') + \mathcal{O}(h^3)\right)u^3 + \mathcal{O}(u^4)$$
(C.17)

It would probably be safe to ignore some of the κ^3 , κ^4 , $\kappa^2\kappa'$, κ'' terms.

$$s = g^{-1}(u) = \left(1 - \frac{h\kappa}{2} + \frac{3h^2\kappa^2}{8}\right)u - \frac{h\kappa'}{6}u^2 + \frac{\kappa^2}{2}u^3 + \mathcal{O}(u^4)$$
 (C.18)

The derivative of this expression is:

$$\frac{\mathrm{d}}{\mathrm{d}u}g^{-1}(u) = 1 - \frac{h\kappa}{2} + \frac{3h^2\kappa^2}{8} - \frac{h\kappa'}{3}u + \frac{3\kappa^2}{2}u^2 + \mathcal{O}(u^3)$$
 (C.19)

Now let f(s, h) be the asymptotic expression for the kernel of interest. We can re-write the above integration as:

$$\int_{-\delta}^{+\delta} f(s,h)\sigma(s) \, ds = \int_{g(-\delta)}^{g(+\delta)} f(g^{-1}(u),h)\sigma(g^{-1}(u)) \, \frac{d}{du}g^{-1}(u) du$$
 (C.20)

Now let's suppose part of the integrand is a second derivative, i.e. $f(g^{-1}(u), h) \frac{d}{du} g^{-1}(u) = \frac{d^2}{du^2} q(u)$. Then we have:

$$\int_{g(-\delta)}^{g(+\delta)} \frac{d^{2}}{du^{2}} q(u) \sigma(g^{-1}(u)) du = \left[\frac{d}{du} q(u) \sigma(g^{-1}(u)) \right]_{g(-\delta)}^{g(+\delta)} - \left[q(u) \frac{d}{du} \sigma(g^{-1}(u)) \right]_{g(-\delta)}^{g(+\delta)} + \int_{g(-\delta)}^{g(+\delta)} q(u) \frac{d^{2}}{du^{2}} \sigma(g^{-1}(u)) du \qquad (C.21)$$

$$= \frac{d^{2}}{du^{2}} \sigma(g^{-1}(u)) \Big|_{u=g(t)} \qquad (C.22)$$

Note that we can write this second derivative as:

$$\frac{\mathrm{d}^2}{\mathrm{d}u^2}\sigma(g^{-1}(u)) = \frac{\mathrm{d}^2\sigma}{\mathrm{d}s^2} \left(\frac{\mathrm{d}s}{\mathrm{d}u}\right)^2 + \frac{\mathrm{d}\sigma}{\mathrm{d}s} \frac{\mathrm{d}^2s}{\mathrm{d}u^2}$$
(C.23)

$$= \frac{\mathrm{d}^2 \sigma}{\mathrm{d}s^2} \left(1 - \frac{h\kappa}{2} + \frac{3h^2\kappa^2}{8} - \frac{5h^3\kappa^3}{16} + \frac{35h^4\kappa^4}{128} + \mathcal{O}(u) \right)^2 \tag{C.24}$$

$$+\frac{\mathrm{d}\sigma}{\mathrm{d}s}\left(-\frac{h\kappa'}{6} + \frac{1}{6}h^2\kappa^2\kappa' - \frac{1}{6}h^3\kappa^4\kappa' + \mathcal{O}(u)\right) \tag{C.25}$$

$$\xrightarrow{h \to 0} \frac{\mathrm{d}^2 \sigma}{\mathrm{d}s^2} \tag{C.26}$$

Let $0 \le m \le n$. Then:

$$\lim_{h \to 0} \int_{-\delta}^{+\delta} \frac{2^n n!}{\pi \prod_{i=1-m}^{n-m} |1 - 2i|} \frac{h^{2(n-m)+1} s^{2m}}{(s^2 + h^2)^{n+1}} \sigma(s) \, \mathrm{d}s = \sigma(t)$$
 (C.27)

Next:

$$\lim_{h \to 0} \int_{-\delta}^{+\delta} \frac{2^n n!}{\pi \prod_{j=1-m}^{n-m} |1-2j|} \left(\frac{2mh^{2(n-m)+1}s^{2m-1}}{(s^2+h^2)^{n+1}} - \frac{2(n+1)h^{2(n-m)+1}s^{2m+1}}{(s^2+h^2)^{n+2}} \right) = -\frac{\mathrm{d}}{\mathrm{d}s} \sigma(s) \big|_{s=t}$$
(C.28)

Finally:

$$\lim_{h \to 0} \int_{-\delta}^{+\delta} \frac{2^{n} n!}{\pi \prod_{j=1-m}^{n-m} |1-2j|} \left(\frac{2m(2m-1)h^{2(n-m)+1}s^{2m-2}}{(s^{2}+h^{2})^{n+1}} - \frac{4m(n+1)h^{2(n-m)+1}s^{2m}}{(s^{2}+h^{2})^{n+2}} - \frac{2(2m+1)(n+1)h^{2(n-m)+1}s^{2m}}{(s^{2}+h^{2})^{n+2}} + \frac{2(n+1)(n+2)h^{2(n-m)+1}s^{2m+2}}{(s^{2}+h^{2})^{n+3}} \right) = \frac{d^{2}}{ds^{2}} \sigma(s) \Big|_{s=t}$$
(C.29)

Given the relations above it is possible to find the jump conditions for all the fifth derivatives, with limits taken from the exterior of the domain:

$$\lim_{\mathbf{x}\to\partial\Omega} \int_{\partial\Omega} G_{n_{\mathbf{x}}n_{\mathbf{x}}n_{\mathbf{y}}n_{\mathbf{y}}n_{\mathbf{y}}}(\mathbf{x},\mathbf{y})\sigma(\mathbf{y}) \,dS(\mathbf{y}) = \left(\frac{\mathrm{d}^{2}}{\mathrm{d}s^{2}} + \frac{1}{2}\kappa^{2}\right)\sigma(\mathbf{x}) + \int_{\partial\Omega} G_{n_{\mathbf{x}}n_{\mathbf{x}}n_{\mathbf{y}}n_{\mathbf{y}}n_{\mathbf{y}}}(\mathbf{x},\mathbf{y})\sigma(\mathbf{y}) \,dS(\mathbf{y})$$
(C.30)
$$\lim_{\mathbf{x}\to\partial\Omega} \int_{\partial\Omega} G_{\tau_{\mathbf{x}}\tau_{\mathbf{x}}n_{\mathbf{y}}n_{\mathbf{y}}n_{\mathbf{y}}}(\mathbf{x},\mathbf{y})\sigma(\mathbf{y}) \,dS(\mathbf{y}) = \left(-\frac{1}{2}\frac{\mathrm{d}^{2}}{\mathrm{d}s^{2}} + \frac{1}{2}\kappa^{2}\right)\sigma(\mathbf{x}) + \int_{\partial\Omega} G_{\tau_{\mathbf{x}}\tau_{\mathbf{x}}n_{\mathbf{y}}n_{\mathbf{y}}n_{\mathbf{y}}}(\mathbf{x},\mathbf{y})\sigma(\mathbf{y}) \,dS(\mathbf{y})$$
(C.31)
$$\lim_{\mathbf{x}\to\partial\Omega} \int_{\partial\Omega} G_{n_{\mathbf{x}}n_{\mathbf{x}}n_{\mathbf{y}}\tau_{\mathbf{y}}\tau_{\mathbf{y}}}(\mathbf{x},\mathbf{y})\sigma(\mathbf{y}) \,dS(\mathbf{y}) = \left(-\frac{1}{2}\frac{\mathrm{d}^{2}}{\mathrm{d}s^{2}} - \frac{1}{2}\kappa^{2}\right)\sigma(\mathbf{x}) + \int_{\partial\Omega} G_{n_{\mathbf{x}}n_{\mathbf{x}}n_{\mathbf{y}}\tau_{\mathbf{y}}\tau_{\mathbf{y}}}(\mathbf{x},\mathbf{y})\sigma(\mathbf{y}) \,dS(\mathbf{y})$$
(C.32)
$$\lim_{\mathbf{x}\to\partial\Omega} \int_{\partial\Omega} G_{\tau_{\mathbf{x}}\tau_{\mathbf{x}}n_{\mathbf{y}}\tau_{\mathbf{y}}\tau_{\mathbf{y}}}(\mathbf{x},\mathbf{y})\sigma(\mathbf{y}) \,dS(\mathbf{y}) = -\frac{1}{2}\kappa^{2}\sigma(\mathbf{x}) + \int_{\partial\Omega} G_{\tau_{\mathbf{x}}\tau_{\mathbf{x}}n_{\mathbf{y}}\tau_{\mathbf{y}}\tau_{\mathbf{y}}}(\mathbf{x},\mathbf{y})\sigma(\mathbf{y}) \,dS(\mathbf{y})$$
(C.33)

For the interior limits, the signs of the identity term will be flipped.

References

- [1] P. Farkas, Mathematical Foundations for Fast Methods for the Biharmonic Equation, Ph.D. thesis, The University of Chicago (1989).
- [2] G. Kirchhoff, Über das gleichgewicht und die bewegung einer elastischen scheibe., Journal für die reine und angewandte Mathematik 40 (1850) 51–88. doi:10.1515/crll.1850.40.51.
- [3] A. E. H. Love, The Small Free Vibrations and Deformation of a Thin Elastic Shell, Philosophical Transactions of the Royal Society of London Series A 179 (1888) 491–546. doi:10.1098/rsta.1888.0016.
- [4] S. Timoshenko, S. Woinowsky-Krieger, et al., Theory of Plates and Shells, Vol. 2, McGraw-hill New York, 1959.
- [5] P. Drábek, G. Holubová, A. Matas, P. Nečesal, Nonlinear Models of Suspension Bridges: Discussion of the Results, Applications of Mathematics 48 (6) (2003) 497–514. doi:10.1023/B:APOM.0000024489. 96314.7f.
- [6] R. A. Massom, T. A. Scambos, L. G. Bennetts, P. Reid, V. A. Squire, S. E. Stammerjohn, Antarctic ice shelf disintegration triggered by sea ice loss and ocean swell, Nature 558 (2018) 383–389. doi: 10.1038/s41586-018-0212-1.
- [7] W. Ritz, Theorie der Transversalschwingungen einer quadratischen Platte mit freien Rändern, Annalen der Physik 333 (4) (1909) 737–786. doi:10.1002/andp.19093330403.

- [8] K. Friedrichs, Die Randwert-und Eigenwertprobleme aus der Theorie der elastischen Platten. (Anwendung der direkten Methoden der Variationsrechnung), Mathematische Annalen 98 (1) (1928) 205a–247. doi:10.1007/BF01451590.
- [9] T. Kato, H. Fujita, Y. Nakata, M. Newman, Estimation of the frequencies of thin elastic plates with free edges, J. Res. Natl. Bur. Stds 59 (1957). doi:10.6028/jres.059.017.
- [10] L. D. Landau, E. M. Lifshitz, Theory of Elasticity, 3rd Edition, Vol. 7, Butterworth-Heinemann, Oxford, 1986. doi:10.1016/B978-0-08-057069-3.50010-3.
- [11] Y. Zhao, G. Wei, Y. Xiang, Plate vibration under irregular internal supports, International Journal of Solids and Structures 39 (5) (2002) 1361–1383. doi:10.1016/S0020-7683(01)00241-4.
- [12] A. Rajamani, R. Prabhakaran, Dynamic response of composite plates with cut-outs, part i: Simply-supported plates, Journal of Sound and Vibration 54 (4) (1977) 549–564. doi:10.1016/0022-460X(77) 90612-5.
- [13] M. Huang, T. Sakiyama, Free vibration analysis of rectangular plates with variously-shaped holes, Journal of Sound and Vibration 226 (4) (1999) 769–786. doi:10.1006/jsvi.1999.2313.
- [14] D. Yu, Y. Liu, H. Zhao, G. Wang, J. Qiu, Flexural vibration band gaps in euler-bernoulli beams with locally resonant structures with two degrees of freedom, Phys. Rev. B 73 (2006) 064301. doi: 10.1103/PhysRevB.73.064301.
- [15] A. E. Lindsay, B. Quaife, L. Wendelberger, A boundary integral equation method for mode elimination and vibration confinement in thin plates with clamped points, Advances in Computational Mathematics 44 (4) (2018) 1249–1273. doi:10.1007/s10444-017-9580-6.
- [16] Z. Zhu, Y. Song, Y. Zhang, Q. Liu, G. Wang, Sound radiation of the plate with arbitrary holes, International Journal of Mechanical Sciences 264 (2024) 108814. doi:10.1016/j.ijmecsci.2023. 108814.
- [17] B. Laulagnet, Sound radiation by a simply supported unbaffled plate, The Journal of the Acoustical Society of America 103 (5) (1998) 2451–2462. doi:10.1121/1.422765.
- [18] P. Monk, A Mixed Finite Element Method for the Biharmonic Equation, SIAM Journal on Numerical Analysis 24 (4) (1987) 737–749. doi:10.1137/0724048.
- [19] A. Climente, D. Torrent, J. Sánchez-Dehesa, Gradient index lenses for flexural waves based on thickness variations, Applied Physics Letters 105 (6) (2014). doi:10.1063/1.4893153.
- [20] D. Mora, R. Rodríguez, A piecewise linear finite element method for the buckling and the vibration problems of thin plates, Mathematics of Computation 78 (268) (2009) 1891–1917. doi:10.1090/S0025-5718-09-02228-5.
- [21] M. H. Meylan, Wave response of an ice floe of arbitrary geometry, Journal of Geophysical Research: Oceans 107 (C1) (2002) 5–1–5–11. doi:10.1029/2000JC000713.
- [22] K. Ishihara, A Mixed Finite Element Method for the Biharmonic Eigenvalue Problems of Plate Bending, Publications of the Research Institute for Mathematical Sciences 14 (2) (1978) 399–414. doi:10.2977/ prims/1195189071.
- [23] Bramble, James H., Falk, Richard S., Two mixed finite element methods for the simply supported plate problem, RAIRO. Anal. numér. 17 (4) (1983) 337–384. doi:10.1051/m2an/1983170403371.
- [24] J. Yue, P. Li, X. Yuan, X. Zhu, A diffraction problem for the biharmonic wave equation in onedimensional periodic structures, Results in Applied Mathematics 17 (2023) 100350. doi:10.1016/j. rinam.2022.100350.
- [25] J. Yue, P. Li, Numerical solution of the cavity scattering problem for flexural waves on thin plates: Linear finite element methods, Journal of Computational Physics 497 (2024) 112606. doi:10.1016/j.jcp.2023.112606.
- [26] M. Farhat, S. Guenneau, S. Enoch, Finite elements modelling of scattering problems for flexural waves in thin plates: Application to elliptic invisibility cloaks, rotators and the mirage effect, Journal of Computational Physics 230 (6) (2011) 2237–2245. doi:10.1016/j.jcp.2010.12.009.
- [27] K. E. Atkinson, The Numerical Solution of Integral Equations of the Second Kind, Cambridge Monographs on Applied and Computational Mathematics, Cambridge University Press, 1997.
- [28] R. Kress, Linear Integral Equations, Applied Mathematical Sciences, Springer, 2014.

- [29] D. Colton, R. Kress, Integral equation methods in scattering theory, SIAM, 2013.
- [30] W. Hackbusch, Numerical Treatment of Fredholm Integral Equations of the Second Kind, Birkhäuser Basel, Basel, 1995, Ch. 4, pp. 59–154. doi:10.1007/978-3-0348-9215-5_4.
- [31] S. Agmon, Multiple layer potentials and the Dirichlet problem for higher order elliptic equations in the plane I, Communications on Pure and Applied Mathematics 10 (2) (1957) 179–239.
- [32] J. Cohen, J. Gosselin, The Dirichlet problem for the biharmonic equation in a C¹ domain in the plane, Indiana University mathematics journal 32 (5) (1983) 635–685.
- [33] N. Muschelišvili, Research on boundary value problems relating to the biharmonic equation and the two-dimensional elasticity equations, Mathematische Annalen 107 (1933) 282–312.
- [34] M. Rachh, T. Askham, Integral Equation Formulation of the Biharmonic Dirichlet Problem, Journal of Scientific Computing 75 (2) (2018) 762–781. doi:10.1007/s10915-017-0559-8.
- [35] G. C. Hsiao, W. L. Wendland, Boundary integral equations, Springer, 2008.
- [36] F. París, S. de León, Simply supported plates by the boundary integral equation method, International Journal for Numerical Methods in Engineering 23 (2) (1986) 173–191. doi:10.1002/nme.1620230202.
- [37] J. Sladek, V. Sladek, H. A. Mang, Meshless formulations for simply supported and clamped plate problems, International Journal for Numerical Methods in Engineering 55 (3) (2002) 359–375. doi: 10.1002/nme.503.
- [38] S. Jiang, B. Ren, P. Tsuji, L. Ying, Second kind integral equations for the first kind Dirichlet problem of the biharmonic equation in three dimensions, Journal of Computational Physics 230 (19) (2011) 7488-7501. doi:10.1016/j.jcp.2011.06.015.
- [39] H. Dong, P. Li, A Novel Boundary Integral Formulation for the Biharmonic Wave Scattering Problem, Journal of Scientific Computing 98 (2) (2024) 42. doi:10.1007/s10915-023-02429-6.
- [40] M. J. Smith, M. H. Meylan, R. C. McPhedran, Scattering by cavities of arbitrary shape in an infinite plate and associated vibration problems, Journal of Sound and Vibration 330 (16) (2011) 4029–4046. doi:10.1016/j.jsv.2011.03.019.
- [41] F. Lakitosh, Analysis of ship hull and plate vibrations caused by wave forces, Florida Atlantic University, 2012.
- [42] R. K. Kapania, Y. Liu, Static and vibration analyses of general wing structures using equivalent-plate models, AIAA journal 38 (7) (2000) 1269–1277.
- [43] G. L. Giles, Further generalization of an equivalent plate representation for aircraft structural analysis, Journal of Aircraft 26 (1) (1989) 67–74. doi:10.2514/3.45724.
- [44] O. V. Sergienko, Normal modes of a coupled ice-shelf/sub-ice-shelf cavity system, Journal of Glaciology 59 (213) (2013) 76–80. doi:10.3189/2013JoG12J096.
- [45] P. Nekrasov, D. R. MacAyeal, Ocean wave blocking by periodic surface rolls fortifies Arctic ice shelves, Journal of Glaciology (2023) 1–11doi:10.1017/jog.2023.58.
- [46] O. V. Sergienko, Behavior of flexural gravity waves on ice shelves: Application to the Ross Ice Shelf, Journal of Geophysical Research: Oceans 122 (8) (2017) 6147–6164. doi:10.1002/2017JC012947.
- [47] P. Friedl, F. Weiser, A. Fluhrer, M. H. Braun, Remote sensing of glacier and ice sheet grounding lines: A review, Earth-Science Reviews 201 (2020) 102948. doi:10.1016/j.earscirev.2019.102948.
- [48] NIST Digital Library of Mathematical Functions, https://dlmf.nist.gov/, Release 1.2.1 of 2024-06-15, f. W. J. Olver, A. B. Olde Daalhuis, D. W. Lozier, B. I. Schneider, R. F. Boisvert, C. W. Clark, B. R. Miller, B. V. Saunders, H. S. Cohl, and M. A. McClain, eds. (2024).
- [49] D. V. Ukrainskii, On the Type of Flexural Edge Wave on a Circular Plate, Mechanics of Solids 53 (5) (2018) 501–509. doi:10.3103/S0025654418080046.
- [50] M. H. Meylan, V. A. Squire, Response of a circular ice floe to ocean waves, Journal of Geophysical Research: Oceans 101 (C4) (1996) 8869–8884. doi:10.1029/95JC03706.
- [51] N. Muskhelishvili, J. Radok, Singular Integral Equations, Noordhoff, Groningen, 1953.
- [52] F. Hang, S. Jiang, Generalized Poincaré-Bertrand formula on a hypersurface, Applied and Computational Harmonic Analysis 27 (1) (2009) 100-116. doi:10.1016/j.acha.2008.12.001.
- [53] P. Seide, Compressive Buckling of a Long Simply Supported Plate on an Elastic Foundation, Journal of the Aerospace Sciences 25 (6) (1958) 382–384. doi:10.2514/8.7691.

- [54] R. T. Walker, B. R. Parizek, R. B. Alley, S. Anandakrishnan, K. L. Riverman, K. Christianson, Ice-shelf tidal flexure and subglacial pressure variations, Earth and Planetary Science Letters 361 (2013) 422–428. doi:10.1016/j.epsl.2012.11.008.
- [55] G. Holdsworth, J. E. Glynn, A mechanism for the formation of large icebergs, Journal of Geophysical Research: Oceans 86 (C4) (1981) 3210–3222. doi:10.1029/JC086iC04p03210.
- [56] M. H. Meylan, M. Ilyas, B. P. Lamichhane, L. G. Bennetts, Swell-induced flexural vibrations of a thickening ice shelf over a shoaling seabed, Proceedings of the Royal Society A: Mathematical, Physical and Engineering Sciences 477 (2254) (2021) 20210173. doi:10.1098/rspa.2021.0173.
- [57] J. Bremer, Z. Gimbutas, V. Rokhlin, A nonlinear optimization procedure for generalized Gaussian quadratures, SIAM Journal on Scientific Computing 32 (4) (2010) 1761–1788.
- [58] T. Askham, M. Rachh, M. O'Neil, J. Hoskins, D. Fortunato, S. Jiang, F. Fryklund, T. Goodwill, H. Y. Wang, H. Zhu, chunkIE: a MATLAB integral equation toolbox (Jun. 2024). URL https://github.com/fastalgorithms/chunkie
- [59] L. Greengard, V. Rokhlin, A fast algorithm for particle simulations, J. Comput. Phys. 73 (2) (1987) 325–348. doi:10.1016/0021-9991(87)90140-9.
- [60] J. Carrier, L. Greengard, V. Rokhlin, A fast adaptive multipole algorithm for particle simulations, SIAM J. Sci. Statist. Comput. 9 (4) (1988) 669–686. doi:10.1137/0909044.
- [61] H. Cheng, L. Greengard, V. Rokhlin, A fast adaptive multipole algorithm in three dimensions, J. Comput. Phys. 155 (2) (1999) 468-498. doi:10.1006/jcph.1999.6355.
- [62] W. Fong, E. Darve, The black-box fast multipole method, J. Comput. Phys. 228 (23) (2009) 8712–8725. doi:10.1016/j.jcp.2009.08.031.
- [63] Z. Gimbutas, V. Rokhlin, A Generalized Fast Multipole Method for Nonoscillatory Kernels, SIAM J. Sci. Comput. 24 (3) (2002) 796–817. doi:10.1137/S1064827500381148.
- [64] L. Greengard, V. Rokhlin, A new version of the Fast Multipole Method for the Laplace equation in three dimensions, in: Acta numerica, 1997, Vol. 6 of Acta Numer., Cambridge Univ. Press, 1997, pp. 229–269. doi:10.1017/S0962492900002725.
- [65] L. Ying, G. Biros, D. Zorin, A kernel-independent adaptive fast multipole algorithm in two and three dimensions, J. Comput. Phys. 196 (2) (2004) 591–626. doi:10.1016/j.jcp.2003.11.021.
- [66] B. Zhang, J. Huang, N. P. Pitsianis, X. Sun, A Fourier-series-based kernel-independent fast multipole method, J. Comput. Phys. 230 (15) (2011) 5807-5821. doi:10.1016/j.jcp.2011.03.049.
- [67] S. Ambikasaran, E. F. Darve., An $O(N \log N)$ fast direct solver for partial hierarchically semi-separable matrices, J. Sci. Comput. 57 (3) (2013) 477–501.
- [68] A. Aminfar, S. Ambikasaran, E. Darve, A fast block low-rank dense solver with applications to finite-element matrices, Journal of Computational Physics 304 (2016) 170–188.
- [69] W. Hackbusch, B. N. Khoromskij, A sparse H-matrix arithmetic: General complexity estimates, J. Comput. Appl. Math. 125 (1) (2000) 479–501. doi:10.1016/S0377-0427(00)00486-6.
- [70] W. Hackbusch, S. Börm, Data-sparse approximation by adaptive H²-matrices, Computing 69 (1) (2002) 1–35.
- [71] W. Hackbusch, S. Börm, H²-matrix approximation of integral operators by interpolation, Appl. Numer. Math. 43 (1) (2002) 129–143.
- [72] S. Chandrasekaran, M. Gu, A fast and stable solver for recursively semi-separable systems of linear equations, in: Structured matrices in mathematics, computer science, and engineering, II (Boulder, CO, 1999), Vol. 281 of Contemp. Math., Amer. Math. Soc., Providence, RI, 2001, pp. 39–53. doi: 10.1090/conm/281/04647.
- [73] Z. Sheng, P. Dewilde, S. Chandrasekaran, Algorithms to solve hierarchically semi-separable systems, in: System theory, the Schur algorithm and multidimensional analysis, Vol. 176 of Oper. Theory Adv. Appl., Birkhäuser, Basel, 2007, pp. 255–294. doi:10.1007/978-3-7643-8137-0_5.
- [74] S. Chandrasekaran, M. Gu, X. Sun, J. Xia, J. Zhu, A superfast algorithm for Toeplitz systems of linear equations, SIAM J. Matrix Anal. Appl. 29 (4) (2007) 1247–1266. doi:10.1137/040617200.
- [75] J. Xia, S. Chandrasekaran, M. Gu, X. S. Li, Superfast multifrontal method for large structured linear systems of equations, SIAM J. Matrix Anal. Appl. 31 (3) (2009) 1382–1411. doi:10.1137/09074543X.

- [76] P. Dewilde, H. Jiao, S. Chandrasekaran, Model reduction in symbolically semi-separable systems with application to pre-conditioners for 3D sparse systems of equations, in: Characteristic functions, scattering functions and transfer functions, Vol. 197 of Oper. Theory Adv. Appl., Birkhäuser Verlag, Basel, 2010, pp. 99–132.
- [77] P.-G. Martinsson, Fast direct solvers for elliptic PDEs, SIAM, 2019.
- [78] J. Bremer, A fast direct solver for the integral equations of scattering theory on planar curves with corners, J. Comput. Phys. 231 (4) (2012) 1879–1899. doi:10.1016/j.jcp.2011.11.015.
- [79] A. Gillman, P. M. Young, P.-G. Martinsson, A direct solver with O(N) complexity for integral equations on one-dimensional domains, Front. Math. China 7 (2) (2012) 217–247. doi:10.1007/s11464-012-0188-3.
- [80] L. Greengard, D. Gueyffier, P.-G. Martinsson, V. Rokhlin, Fast direct solvers for integral equations in complex three-dimensional domains, Acta Numer. 18 (2009) 243–275. doi:10.1017/S0962492906410011.
- [81] K. L. Ho, L. Greengard, A fast direct solver for structured linear systems by recursive skeletonization, SIAM J. Sci. Comput. 34 (5) (2012) A2507–A2532. doi:10.1137/120866683.
- [82] W. Y. Kong, J. Bremer, V. Rokhlin, An adaptive fast direct solver for boundary integral equations in two dimensions, Appl. Comput. Harmon. Anal. 31 (3) (2011) 346–369. doi:10.1016/j.acha.2011.01.008.
- [83] P. G. Martinsson, A fast direct solver for a class of elliptic partial differential equations, J. Sci. Comput. 38 (3) (2009) 316–330. doi:10.1007/s10915-008-9240-6.
- [84] P. G. Martinsson, V. Rokhlin, A fast direct solver for boundary integral equations in two dimensions, J. Comput. Phys. 205 (1) (2005) 1–23. doi:10.1016/j.jcp.2004.10.033.
- [85] P. G. Martinsson, V. Rokhlin, A fast direct solver for scattering problems involving elongated structures, J. Comput. Phys. 221 (1) (2007) 288–302. doi:10.1016/j.jcp.2006.06.037.
- [86] G. R. Marple, A. Barnett, A. Gillman, S. Veerapaneni, A Fast Algorithm for Simulating Multiphase Flows Through Periodic Geometries of Arbitrary Shape, SIAM Journal on Scientific Computing 38 (5) (2016) B740–B772. doi:10.1137/15M1043066.
- [87] V. Minden, K. L. Ho, A. Damle, L. Ying., A recursive skeletonization factorization based on strong admissibility, SIAM Multiscale Model. Simul. 69 (2017) 1415–1451. doi:10.1137/16M1095949.
- [88] J. Bremer, A. Gillman, P.-G. Martinsson, A high-order accurate accelerated direct solver for acoustic scattering from surfaces, BIT Numerical Mathematics 55 (2015) 367–397. doi:10.1007/ s10543-014-0508-y.
- [89] A. Gopal, P.-G. Martinsson, An accelerated, high-order accurate direct solver for the lippmann–schwinger equation for acoustic scattering in the plane, Advances in Computational Mathematics 48 (4) (2022) 42. doi:10.1007/s10444-022-09963-1.
- [90] K. Jose, N. Ferguson, A. Bhaskar, Branched flows of flexural waves in non-uniform elastic plates, Communications Physics 5 (1) (2022) 152. doi:10.1038/s42005-022-00917-z.
- [91] K. Jose, N. Ferguson, A. Bhaskar, Branched flows of flexural elastic waves in non-uniform cylindrical shells, PLOS ONE 18 (5) (2023) 1–15. doi:10.1371/journal.pone.0286420.
- [92] T. J. Matula, P. L. Marston, Energy branching of a subsonic flexural wave on a plate at an air-water interface. I. Observation of the wave field near the interface and near the plate, The Journal of the Acoustical Society of America 97 (3) (1995) 1389–1398. doi:10.1121/1.412081.
- [93] A. Darabi, A. Zareei, M.-R. Alam, M. J. Leamy, Broadband Bending of Flexural Waves: Acoustic Shapes and Patterns, Scientific Reports 8 (1) (2018) 11219. doi:10.1038/s41598-018-29192-1.
- [94] L. Zhao, A. Barnett, Robust and efficient solution of the drum problem via Nystrom approximation of the Fredholm determinant, SIAM Journal on Numerical Analysis 53 (4) (2015) 1984–2007. doi: 10.1137/140973992.
- [95] T. Askham, M. Rachh, A boundary integral equation approach to computing eigenvalues of the stokes operator, Advances in Computational Mathematics 46 (2) (2020) 20. doi:10.1007/s10444-020-09774-2.
- [96] A. F. Banwell, J. C. Burton, C. Cenedese, K. Golden, J. Åström, Physics of the cryosphere, Nature Reviews Physics 5 (8) (2023) 446–449. doi:10.1038/s42254-023-00610-2.

- [97] M. O'Neil, L. Greengard, A. Pataki, On the efficient representation of the half-space impedance Green's function for the Helmholtz equation, Wave Motion 51 (1) (2014) 1–13. doi:10.1016/j.wavemoti. 2013.04.012.
- [98] A. Sommerfeld, Partial Differential Equations in Physics, Academic Press, 1949. doi:10.1016/B978-0-12-654658-3.X5001-0.